




Controlling gain with loss: Bounds on localizable entanglement in multiqubit systems

Jithin G. Krishnan , Harikrishnan K. J. , and Amit Kumar Pal 

Department of Physics, Indian Institute of Technology Palakkad, Palakkad 678 623, India



(Received 16 September 2022; accepted 8 March 2023; published 10 April 2023)

We investigate the relation between the amount of entanglement localized on a chosen subsystem of a multiqubit system via local measurements on the rest of the system, and the bipartite entanglement that is lost during this measurement process. We study a number of paradigmatic pure states, including the generalized Greenberger–Horne–Zeilinger (GHZ), the generalized W (gW), Dicke, and the generalized Dicke states. For the generalized GHZ and W states, we analytically derive bounds on localizable entanglement in terms of the entanglement present in the system prior to the measurement. Also, for the Dicke and the generalized Dicke states, we demonstrate that with increasing system size, localizable entanglement tends to be equal to the bipartite entanglement present in the system over a specific partition before measurement. We extend the investigation numerically in the case of arbitrary multiqubit pure states. We also analytically determine the modification of these results, including the proposed bounds, in situations where these pure states are subjected to single-qubit phase-flip noise on all qubits. Additionally, we study one-dimensional paradigmatic quantum spin models, namely, the transverse-field XY model and the XXZ model in an external field, and numerically demonstrate a cubic dependence of the localized entanglement on the lost entanglement. We show that this relation is robust even in the presence of disorder in the strength of the external field.

DOI: [10.1103/PhysRevA.107.042411](https://doi.org/10.1103/PhysRevA.107.042411)

I. INTRODUCTION

In the last three decades, entanglement [1,2] has been established as the key resource in quantum information processing tasks, including quantum teleportation [1,3,4], superdense coding [1,5–7], and quantum cryptography [8,9]. Concepts related to entanglement theory have also been used in areas that are seemingly different from quantum information theory, such as in probing gauge-gravity duality [10–13], in understanding time as an emergent phenomena from entanglement [14–16], and even in studying systems like photosynthetic complexes [17] that are important from a biological point of view. These have motivated enormous experimental advancements in creating and manipulating entangled states in the laboratory using various substrates, namely, photons [18–20], trapped ions [21–23], cold atoms [24–26], superconducting qubits [27,28], and nuclear magnetic resonance molecules [29]. Moreover, quantum many-body systems [30] have emerged as the natural choice for implementing quantum information processing tasks, and the necessity of studying the entanglement properties of these systems has also been realized [31,32].

Entanglement over a subsystem A of a composite quantum system in state ρ can be quantified by computing an appropriate entanglement measure E over the reduced state $\rho_A = \text{Tr}_B[\rho]$ of the subsystem A , where B is the rest of the system [1,2]. While this approach has been successful in a wide variety of multipartite quantum states [1,2,33], there exist states like N -qubit Greenberger–Horne–Zeilinger (GHZ) states [34], graph states [35], and stabilizer states in quantum error correcting codes [36,37] for which the *partial trace-based* avenue may lead to a vanishing entanglement measure on state ρ_A . In such situations, one may take a *measurement-based* approach,

where nonzero bipartite or multipartite entanglement can be *localized* on subsystem A in the postmeasured state of the system by performing measurements on B [38]. In the case of a multiqubit system, this leads to the definition of the localizable entanglement [39–41], defined as the maximum average entanglement localized over A via local single-qubit projection measurements on all qubits in B , given by

$$\langle E_A \rangle = \max_k \sum_k p_k E(\tilde{\rho}_A^k). \quad (1)$$

Here, k labels the measurement outcomes corresponding to the postmeasured states $\tilde{\rho}^k$ occurring with probability p_k ($\sum_k p_k = 1$), where $\tilde{\rho}_A^k = \text{Tr}_B[\tilde{\rho}^k]$. Depending on the possible partitions in A , the entanglement measure E computed over A postmeasurement can be either a bipartite [39–41] or a multipartite [42] measure. Apart from successfully characterizing entanglement in GHZ and GHZ-like states such as the graph [35] and the stabilizer states [43,44], localizable entanglement and related ideas have been immensely useful in defining the correlation length in one-dimensional (1D) quantum spin models [39–41,45], in characterizing quantum phase transitions in the cluster-Ising [46,47] and cluster-XY models [48] in terms of entanglement, and in entanglement percolation through quantum networks [49].

The measurement on subsystem B completely decouples B from A , leading to

$$\rho \rightarrow \tilde{\rho} = \tilde{\rho}_A \otimes \tilde{\rho}_B, \quad (2)$$

implying a complete loss in entanglement over all qubits belonging to the different subsystems A and B . A natural question that arises is whether and how the entanglement $\langle E_A \rangle$ localized on A via measurements on B depends on the entanglement that is lost during the same measurement

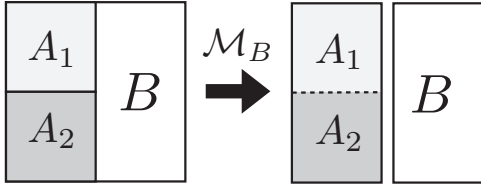


FIG. 1. Consider a multiqubit system divided into three subsystems, A_1 , A_2 , and B , with bipartite entanglement $E_{A_1A_2:B}$, $E_{A_1:A_2B}$, and $E_{A_2:A_1B}$ over different bipartitions. Measurement on all qubits in B , denoted by \mathcal{M}_B , decouples the subsystem B from the qubits in $A \equiv A_1A_2$.

process. More specifically, considering a bipartition $A_1 : A_2$ of A (i.e., an overall tripartition $A_1 : A_2 : B$ of the multiqubit system, see Fig. 1) and a bipartite entanglement measure E , we ponder the following question: Does any relation exist between the bipartite entanglement $\langle E_A \rangle \equiv \langle E_{A_1A_2} \rangle$ localized over subsystem A via single-qubit projection measurements on all qubits in B , and the entanglement over different bipartitions prior to the measurement, namely, $E_{A_1A_2:B}$, $E_{A_1:A_2B}$, and $E_{A_2:A_1B}$, that are lost during the measurement process leading to $\langle E_{A_1A_2} \rangle$? On one hand, the answer to this question may give rise to constraints on the entanglement localizable over the subsystem of a multiqubit system in terms of the entanglement present in the system prior to measurement—a situation that is of fundamental interest from the perspective of complete characterization of the system via entanglement. On the other hand, such a study may also aid in estimating the localizable entanglement prior to the measurement via the information on the bipartite entanglement present in the system. The latter is advantageous from a practical point of view, especially in situations where performing the measurements and optimizing over all possible measurements may turn out to be difficult.

A few results exist in this direction. Note that the monotonicity of E [1,33,50–52] implies that

$$\langle E_{A_1A_2} \rangle \leq \min [E_{A_1:A_2B}, E_{A_2:A_1B}]. \quad (3)$$

It has been shown that the inequality (3) can be tightened to an equality in the case of asymptotic pure-state distillation [53,54]. At the single copy level, it has also been shown that for all three-qubit pure states with each of A_1 , A_2 , and B being a qubit, the inequality (3) becomes an equality via some measurement on B for a specific choice of entanglement measure [55]. In the case of multiqubit pure states, investigation on the relation between localizable multipartite entanglement $\langle E_A \rangle$ and the multipartite entanglement, as quantified by the multiparty entanglement measure E , over the state prior to the measurement has also been made [42]. However, we are still far from a systematic and complete understanding of the problem in the case of arbitrary multiqubit quantum states.

In this paper, we study the interplay between $\langle E_{A_1A_2} \rangle$, $E_{A_1:A_2B}$, $E_{A_2:A_1B}$, and $E_{A_1A_2:B}$ in multiqubit systems, where each of the partitions A_1 , A_2 , and B may consist of multiple qubits. We start with the investigation of a number of paradigmatic N -qubit pure states, including the generalized GHZ states [34,56], the generalized W states [56,57], Dicke states [58–61], and generalized Dicke (gD) states [42], and analytically derive bounds of $\langle E_{A_1A_2} \rangle$ in terms of $E_{A_1:A_2B}$, $E_{A_2:A_1B}$,

and $E_{A_1A_2:B}$. In the cases of arbitrary pure states of N qubits, we numerically investigate whether it is always possible to exceed the loss in bipartite entanglement via localizations performed through measurement. We extend our investigation to the pure states subjected to the single-qubit phase flip noise [62,63] of the Markovian [64] and non-Markovian [65–67] type, and discuss the modifications of the bounds obtained for pure states due to the presence of noise. We also look into the ground states obtained from 1D interacting quantum spin models, both in the presence and absence of disorder [68]. More specifically, we consider the 1D transverse-field XY (TXY) model [69–74] and the 1D XXZ model in an external field [75–80], where disorder can be present in the strength of the field. We numerically demonstrate a cubic dependence of the localizable entanglement on the entanglement lost during measurement in the ground states of the ordered and the disordered models, and demonstrate that the relation is robust against the presence of disorder in the field strength.

The rest of the paper is organized as follows. In Sec. II, we formally define the localizable entanglement and compute it, along with the bipartite entanglements present in the unmeasured states, in the case of paradigmatic multiqubit pure states. We also present the numerical data corresponding to arbitrary N -qubit pure states and discuss the implications of the data. The modifications of the results for the pure state due to subjecting the states to single-qubit Markovian and non-Markovian phase flip channels are discussed in Sec. III. The study of the localizable and the lost entanglement in the ground states of ordered and disordered 1D quantum spin models can be found in Sec. IV. Section V presents the outlook and concluding remarks.

II. MULTIQUBIT PURE STATES

In this section, we explore a number of paradigmatic multiqubit pure states and discuss the correlation between the localizable entanglement and the bipartite entanglement that is lost due to measurement. Let us take an N -qubit system, S , where the qubits are labeled $1, 2, \dots, N$. As discussed in Sec. I, we consider a tripartition $A_1 : A_2 : B$ of the system, and perform single-qubit rank-1 projection measurements on all qubits in B . Without any loss in generality, we assume that B holds $n (< N - 1)$ qubits, and $A = A_1 \cup A_2$ consists of the rest $N - n$ qubits. We label the qubits in B as $1, 2, \dots, n$, and the qubits in A as $n + 1, n + 2, \dots, N - 1, N$. In this situation, $\langle E_{A_1A_2} \rangle$ [Eq. (1)] takes the form

$$\langle E_{A_1A_2} \rangle = \max \sum_{k=0}^{2^n-1} p_k E(\tilde{\rho}_{A_1A_2}^k), \quad (4)$$

where $\tilde{\rho}_{A_1A_2}^k = \text{Tr}_B[\tilde{\rho}^k]$, $\tilde{\rho}^k = [M^k \rho M^{k\dagger}] / p_k$, and $p_k = \text{Tr}[M^k \rho M^{k\dagger}]$, with M^k being the measurement operation corresponding to the measurement outcome k , and the maximization is performed over the set of all possible single-qubit rank-1 projection measurements on all qubits in B . Note that the maximum value of $\langle E_{A_1A_2} \rangle$ cannot exceed the maximum value of the chosen entanglement measure, E_{\max} , implying $\langle E_{A_1A_2} \rangle \leq E_{\max}$.

The measurement operators $\{M^k\}$ can be written as $M^k = I_{A_1A_2} \otimes P_B^k$, with the projectors on the qubits in B

corresponding to the measurement outcome k given by $P_B^k = |\tilde{b}_k\rangle\langle\tilde{b}_k|$, where $k_i = 0, 1$ and $k \equiv k_1 k_2 \cdots k_n$ is a multi-index. Here, $|\tilde{b}_k\rangle = \otimes_{i \in B} |b_{k_i}\rangle$, and

$$\begin{aligned} |b_0\rangle_i &= \cos \frac{\theta_i}{2} |0\rangle + e^{i\phi_i} \sin \frac{\theta_i}{2} |1\rangle, \\ |b_1\rangle_i &= \sin \frac{\theta_i}{2} |0\rangle - e^{i\phi_i} \cos \frac{\theta_i}{2} |1\rangle \end{aligned} \quad (5)$$

on all qubits $i \in B$, where $\theta_i, \phi_i \in \mathbb{R}$, $0 \leq \theta_i \leq \pi$, $0 \leq \phi \leq 2\pi$. Unless otherwise stated, we maintain these notations in all subsequent calculations. Also, we use A and $A_1 A_2$ interchangeably, since $A \equiv A_1 \cup A_2 = A_1 A_2$.

The maximum value of $\langle E_{A_1 A_2} \rangle$ as well as the optimal measurement basis on B providing this value depends on the choice of E . Therefore, a discussion on the choice of E is in order here. Note that the analytical determination of bounds reported in this as well as in the subsequent sections depends on the computability of the entanglement measure in terms of the state parameters. Also, a computable measure for mixed states is desired as required in the case of noisy systems, discussed in Sec. III. In view of these, we choose negativity [81–85] (see Appendix A for a brief definition) as the entanglement measure for demonstration of the results, although it is important to remind ourselves that negativity, by definition, does not take into account entangled states with positive partial transpose. Therefore, it cannot provide the full picture in the $\mathbb{C}^{d_1} \otimes \mathbb{C}^{d_2}$ scenario except the case of $\mathbb{C}^2 \otimes \mathbb{C}^2$ and $\mathbb{C}^2 \otimes \mathbb{C}^3$ [86–88]. We have also tested our results for other entanglement measures, such as logarithmic negativity [89] and von Neumann entropy [1,2,82,90,91] (see Appendix A for brief definitions), and have found the results to be qualitatively valid. We comment on the subtle differences for different measures as we discuss the specific results in this section and in the subsequent sections.

A. Generalized GHZ states

We start with the N -qubit generalized GHZ (gGHZ) state [34], given by

$$|\text{gGHZ}\rangle = a_0 |0\rangle^{\otimes N} + a_1 |1\rangle^{\otimes N}, \quad (6)$$

where a_0 and a_1 are complex numbers, i.e., $a_0, a_1 \in \mathbb{C}$, and the state is normalized, implying $|a_0|^2 + |a_1|^2 = 1$. For the gGHZ state, we present the following proposition.

Proposition 1. For any tripartition $A_1 : A_2 : B$ of an N -qubit gGHZ state,

$$\langle E_{A_1 A_2} \rangle = E_{A_1 A_2 : B} = E_{A_1 : A_2 B} = E_{A_2 : A_1 B}. \quad (7)$$

Proof. Partial transposition of $\rho = |\text{gGHZ}\rangle\langle\text{gGHZ}|$ with respect to the subsystems B leads to

$$\begin{aligned} \rho^{T_B} &= |a_0|^2 (|0\rangle\langle 0|)^{\otimes N} + |a_1|^2 (|1\rangle\langle 1|)^{\otimes N} \\ &\quad + a_0 a_1^* (|0\rangle\langle 1|)^{\otimes N-n} (|1\rangle\langle 0|)^{\otimes n} \\ &\quad + a_0^* a_1 (|1\rangle\langle 0|)^{\otimes N-n} (|0\rangle\langle 1|)^{\otimes n}, \end{aligned} \quad (8)$$

with nonzero eigenvalues $|a_0|^2, |a_1|^2, \pm |a_0| |a_1|$. Therefore, the entanglement between partition $A_1 A_2$ and partition B , as quantified by negativity, is given by

$$E_{A_1 A_2 : B} = 2|a_0| \sqrt{1 - |a_0|^2}. \quad (9)$$

We now compute localizable entanglement, $\langle E_{A_1 A_2} \rangle$, for the gGHZ state. Application of the measurement operator M^k corresponding to the measurement outcome k on $|\text{gGHZ}\rangle$ leads to

$$M^k |\text{gGHZ}\rangle = |\text{gGHZ}_k\rangle_{A_1 A_2} \otimes |\tilde{b}_k\rangle_B, \quad (10)$$

where

$$\begin{aligned} |\text{gGHZ}_k\rangle &= \frac{1}{\sqrt{p_k}} (a_0 f_0^k |0\rangle^{\otimes(N-n)} + a_1 f_1^k |1\rangle^{\otimes(N-n)}), \\ p_k &= |a_0|^2 |f_0^k|^2 + |a_1|^2 |f_1^k|^2. \end{aligned} \quad (11)$$

Here,

$$\begin{aligned} f_0^k &= \prod_{i \in B} f_0^{k_i} = \prod_{i \in B} \langle b_{k_i} | 0 \rangle_i, \\ f_1^k &= \prod_{i \in B} f_1^{k_i} = \prod_{i \in B} \langle b_{k_i} | 1 \rangle_i \end{aligned} \quad (12)$$

are functions of $2n$ real parameters $\{\theta_i, \phi_i\}$, $i = 1, \dots, n$. The negativity, $E_{A_1 : A_2}^k$, can now be computed for each postmeasured state $|\text{gGHZ}_k\rangle$ on $A_1 A_2$ as

$$E_{A_1 : A_2}^k = \frac{2|a_0| \sqrt{1 - |a_0|^2} |f_0^k| |f_1^k|}{p_k}. \quad (13)$$

The localizable entanglement across the bipartition $A_1 : A_2$ of A is, therefore,

$$\langle E_{A_1 : A_2} \rangle = 2|a_0| \sqrt{1 - |a_0|^2} \left[\max_{k=0}^{2^n-1} |f_0^k| |f_1^k| \right]. \quad (14)$$

To perform the maximization, we note that $|f_{0,1}^k|$, and subsequently p_k and $E_{A_1 : A_2}^k$, are independent of $\{\phi_i\}$, $i = 1, \dots, n$, thereby reducing the maximization problem to one involving n real parameters, $\{\theta_i\}$, $i = 1, \dots, n$. Moreover, since $|f_{0,1}^k| \geq 0$, and

$$|f_0^k| |f_1^k| = \frac{1}{2^n} \prod_{i \in B} \sin \theta_i, \quad (15)$$

one obtains

$$\begin{aligned} \max_{\theta_i} \sum_{k=0}^{2^n-1} |f_0^k| |f_1^k| &= \frac{1}{2^n} \sum_{k=0}^{2^n-1} \max_{\theta_i} \prod_{i \in B} \sin \theta_i \\ &= 1, \end{aligned} \quad (16)$$

where the maximization takes place for $\theta_i = \frac{\pi}{2} \forall i \in B$, implying that a σ^x measurement on all qubits in B is optimal for obtaining the maximum $\langle E_{A_1 A_2} \rangle$ as

$$\langle E_{A_1 A_2} \rangle = 2|a_0| \sqrt{1 - |a_0|^2}. \quad (17)$$

It is easy to see from the symmetry of the gGHZ state that $E_{A_1 A_2 : B} = E_{A_1 : A_2 B} = E_{A_2 : A_1 B}$, leading to

$$\langle E_{A_1 A_2} \rangle = E_{A_1 A_2 : B} = E_{A_1 : A_2 B} = E_{A_2 : A_1 B}. \quad (18)$$

Hence the proof. ■

Therefore, in the case of the N -qubit gGHZ states, it is not possible to exceed the bipartite entanglement present in the state prior to the measurement via localizable entanglement. Note also that for the N -qubit gGHZ state, (3) is an equality.

Also, one can use von Neumann entropy to compute entanglement in the case of the pure gGHZ states, where Eq. (18) is found to be unaltered.

B. Generalized W states

Next, we focus on the N -qubit generalized W states [56,57], given by

$$|gW\rangle = \sum_{i=1}^N a_i |0\rangle^{\otimes(i-1)} |1\rangle_i |0\rangle^{\otimes(N-i)}, \quad (19)$$

where $a_i \in \mathbb{C} \forall i \in \{1, 2, \dots, N\}$, satisfying the normalization condition $\sum_{i=1}^N |a_i|^2 = 1$. Let us first consider a subset of the N -qubit gW states given in Eq. (19) where the coefficients a_i are real, i.e., $a_i \in \mathbb{R}$. We first focus on the correlation between $\langle E_{A_1 A_2} \rangle$ and $E_{A_1 A_2 : B} \equiv E_{AB}$. Negativity over any bipartition AB of the system is given by¹

$$E_{A_1 A_2 : B} = 2 \left| \left[\left(\sum_{i=n+1}^{n+m} a_i^2 + \sum_{i=n+m+1}^N a_i^2 \right) \sum_{i=1}^n a_i^2 \right]^{\frac{1}{2}} \right|, \quad (20)$$

where we have assumed that qubits $1, 2, \dots, n$ constitute the subsystem B , and qubits $n+1, n+2, \dots, N$ form the subsystem B . On the other hand, computation of $\langle E_{A_1 A_2} \rangle$ involves application of $M^k, k = 0, 1, \dots, 2^n - 1$, on the n qubits in B of $|gW\rangle$ (see Sec. II A), leading to

$$M^k |gW\rangle = |\tilde{b}_k\rangle_B \otimes |\psi_k\rangle_{A_1 A_2}, \quad (21)$$

with

$$|\psi_k\rangle = c_0^k |0\rangle^{\otimes(N-n)} + \sum_{i=1}^{N-n} c_i^k |0\rangle^{\otimes(i-1)} |1\rangle_i |0\rangle^{\otimes(N-n-i)}, \quad (22)$$

where $c_0^k = f_0^k / \sqrt{p_k}$, and $c_i^k = f^k a_{n+i} / \sqrt{p_k}$, $i = 1, 2, \dots, N-n$, with p_k being the probability of obtaining the measurement outcome k , such that $\sum_{i=0}^{N-n} |c_i^k|^2 = 1$ ensuring normalization. Note further that among the coefficients $c_i^k, i = 0, 1, \dots, N-n$, only c_0^k is complex (see Appendix B for explicit examples with the cases of single- and two-qubit measurements). Using this, negativity in the state $|\psi_k\rangle$ over the bipartition $A_1 : A_2$ can be written for all k as²

$$E_{A_1 A_2}^k = \frac{2(f^k)^2}{p_k} \left| \left[\left(\sum_{i=n+1}^{n+m} a_i^2 \right) \sum_{i=n+m+1}^N a_i^2 \right]^{\frac{1}{2}} \right|. \quad (23)$$

¹For gW states with real coefficients, this can be obtained by observing the patterns of the negative eigenvalues of the partially transposed density matrix of the smaller systems. Equation (20) is also verified numerically for large gW states with real coefficients as well as complex coefficients, where in the case of the latter, a_i^2 is replaced by $|a_i|^2$.

²This expression for negativity of the states of the form in Eq. (22) has also been obtained analytically for smaller systems and has been verified numerically for larger systems.

Here, we have assumed, without any loss in generality, that the subsystem A_1 (A_2) is constituted of the qubits $n+1, n+2, \dots, n+m$ (qubits $n+m+1, n+m+2, \dots, N$). Therefore,

$$\begin{aligned} \langle E_{A_1 A_2} \rangle &= \sum_k p_k E_{A_1 A_2}^k \\ &= 2 \left| \left[\left(\sum_{i=n+1}^{n+m} a_i^2 \right) \sum_{i=n+m+1}^N a_i^2 \right]^{\frac{1}{2}} \right| \sum_k (f^k)^2. \end{aligned} \quad (24)$$

For small values of n , it can analytically be shown that the factor $\sum_{k=0}^{2^n-1} (f^k)^2 = 1^3$, while our numerical investigation shows this to be true for high values of n also. This leads to

$$\langle E_{A_1 A_2} \rangle = 2 \left| \left[\left(\sum_{i=n+1}^{n+m} a_i^2 \right) \sum_{i=n+m+1}^N a_i^2 \right]^{\frac{1}{2}} \right|. \quad (25)$$

We now propose the following for an N -qubit gW state with real coefficients.

Proposition II. In the space $(E_{A_1 A_2 : B}, \langle E_{A_1 A_2} \rangle)$, the localizable entanglement $\langle E_{A_1 A_2} \rangle$ of an N -qubit normalized gW state with real coefficients is upper bounded by the line

$$\langle E_{A_1 A_2} \rangle = \frac{1}{2} (1 + \sqrt{1 - E_{A_1 A_2 : B}^2}), \quad (26)$$

where $E_{A_1 A_2 : B}$ is the bipartite entanglement over the bipartition $A_1 A_2 : B$ in the state prior to measurement on all the qubits in B .

Proof. For ease of calculation, we focus on $\langle E_{A_1 A_2} \rangle^2$ given by [using Eq. (25) and normalization of the gW state],

$$\langle E_{A_1 A_2} \rangle^2 = 4 \left(1 - \sum_{i=1}^n a_i^2 - \sum_{i=n+1}^{n+m} a_i^2 \right) \sum_{i=n+1}^{n+m} a_i^2, \quad (27)$$

which, for fixed $a = \sum_{i=1}^n a_i^2$, is a single-parameter function $F(x) = 4x(1-a-x)$ of x , where $x \equiv \sum_{i=n+1}^{n+m} a_i^2$. The function $F(x)$ has the maximum value $(1-a)^2$, occurring at $x = (1-a)/2$. This implies $\sum_{i=n+1}^{n+m} a_i^2 = (1-a)/2$ for the maximum of $\langle E_{A_1 A_2} \rangle = 1-a$. Note also from Eq. (20) that $E_{A_1 A_2 : B} = 2\sqrt{a(1-a)}$. Eliminating a and subsequently solving for $\langle E_{A_1 A_2} \rangle$, one obtains Eq. (26). ■

The following corollaries can be obtained straightforwardly from Proposition I.

Corollary II.1. The family of gW states with real coefficients that satisfy Eq. (26) is given by

$$\sum_{i=n+1}^{n+m} a_i^2 = \sum_{i=n+m+1}^N a_i^2 = \frac{1}{2} \left(1 - \sum_{i=1}^n a_i^2 \right). \quad (28)$$

Proof. For a fixed value of $\sum_{i=1}^n a_i^2$, the maximization condition for $\langle E_{A_1 A_2} \rangle$ is given by $\sum_{i=n+1}^{n+m} a_i^2 = \frac{1}{2} (1 - \sum_{i=1}^n a_i^2)$. From the normalization of the gW states, Eq. (28) follows. ■

Corollary II.2. For the family of gW states given by Eq. (28), $E_{A_1 : A_2 B} = E_{A_2 : A_1 B}$.

³See Appendix B for cases up to $n = 2$.

Proof. Similar to Eq. (20), entanglement over the bipartitions $A_2 : A_1B$ and $A_1 : A_2B$ can be written as

$$E_{A_1:A_2B} = 2 \left| \left[\left(\sum_{i=1}^n a_i^2 + \sum_{i=n+m+1}^N a_i^2 \right) \sum_{i=n+1}^{n+m} a_i^2 \right]^{\frac{1}{2}} \right| \quad (29)$$

and

$$E_{A_2:A_1B} = 2 \left| \left[\left(\sum_{i=1}^n a_i^2 + \sum_{i=n+1}^{n+m} a_i^2 \right) \sum_{i=n+m+1}^N a_i^2 \right]^{\frac{1}{2}} \right|, \quad (30)$$

respectively. Clearly, for $\sum_{i=n+1}^{n+m} a_i^2 = \sum_{i=n+m+1}^N a_i^2$, $E_{A_1:A_2B} = E_{A_2:A_1B}$. ■

Proposition III. In $(\min\{E_{A_1:A_2B}, E_{A_2:A_1B}\}, \langle E_{A_1A_2} \rangle)$ space, the localizable entanglement $\langle E_{A_1A_2} \rangle$ of an N -qubit normalized gW state with real coefficients is upper bounded by the line

$$\langle E_{A_1A_2} \rangle = \min\{E_{A_1:A_2B}, E_{A_2:A_1B}\}, \quad (31)$$

and lower-bounded by the line

$$\langle E_{A_1A_2} \rangle^2 - 2\langle E_{A_1A_2} \rangle + (\min\{E_{A_1:A_2B}, E_{A_2:A_1B}\})^2 = 0, \quad (32)$$

where $E_{A_1:A_2B}$ ($E_{A_2:A_1B}$) is the bipartite entanglement over the bipartition $A_1 : A_2B$ ($A_2 : A_1B$) in the state prior to measurement on all the qubits in B .

Proof. The upper bound follows from the monotonicity of E [see Eq. (3)]. On the other hand, note that from Eqs. (29) and (30),

$$E_{A_1:A_2B}^2 = 4 \left(\sum_{i=n+1}^{n+m} a_i^2 \right) \sum_{i=1}^n a_i^2 + \langle E_{A_1A_2} \rangle^2 \quad (33)$$

and

$$E_{A_2:A_1B}^2 = 4 \left(\sum_{i=n+m+1}^N a_i^2 \right) \sum_{i=1}^n a_i^2 + \langle E_{A_1A_2} \rangle^2, \quad (34)$$

respectively, where we have used Eq. (25). Let us proceed by assuming $E_{A_2:A_1B} \geq E_{A_1:A_2B}$, implying $\min\{E_{A_1:A_2B}, E_{A_2:A_1B}\} = E_{A_1:A_2B}$, and $\sum_{i=n+m+1}^N a_i^2 \geq \sum_{i=n+1}^{n+m} a_i^2$. For a fixed $a = \sum_{i=n+1}^{n+m} a_i^2$, $\langle E_{A_1A_2} \rangle$ is minimum if $\sum_{i=n+m+1}^N a_i^2$ is minimum, leading to $\sum_{i=n+m+1}^N a_i^2 = a$, and subsequently $\langle E_{A_1A_2} \rangle \geq 2a$ and $E_{A_1:A_2B} = 2\sqrt{a(1-a)}$. Eliminating a , we obtain the equation of the lower bound as

$$\langle E_{A_1A_2} \rangle^2 - 2\langle E_{A_1A_2} \rangle + E_{A_1:A_2B}^2 = 0. \quad (35)$$

Similarly, assuming $E_{A_1:A_2B} \geq E_{A_2:A_1B}$, one can also prove that

$$\langle E_{A_1A_2} \rangle^2 - 2\langle E_{A_1A_2} \rangle + E_{A_2:A_1B}^2 = 0. \quad (36)$$

Equations (35) and (36) lead to Eq. (32). ■

Note 1. Note here that Propositions II and III and the related corollaries are proved for the subclass of gW states with real coefficients, and it is therefore logical to ask whether the same results apply to the gW states with complex coefficients. While analytical calculation is difficult for a generic N -qubit gW state due to increase in the number of state parameters, for demonstration, we perform the calculation for the gW state with $N = 3$, and find Propositions II and III and the corollaries

to be unchanged (see Appendix C). We also numerically check the applicability of these results for N -qubit gW states with arbitrary N and complex coefficients and find them to be valid. Therefore, for generic gW states, Propositions II, III and Corollaries II.1 and II.2 can be straightforwardly updated by replacing a_i^2 with $|a_i|^2$ for all $i = 1, \dots, N$. For demonstrations of these results, see Figs. 2(a) and 2(b). Specific examples of the family of states described in Eq. (28) can be found in Appendix D.

Note 2. Note in Fig. 2(a) that apart from the line given by Eq. (26), the Haar uniformly [92,93] chosen gW states are also bounded by the lines (a) $E_{A_1A_2:B} = 0$, (b) $\langle E_{A_1A_2} \rangle = 0$, and (c) $E_{A_1A_2:B} = 1$, which are not shown explicitly in the figure, and which are obtained from the fact that $0 \leq E_{A_1A_2:B}, \langle E_{A_1A_2} \rangle \leq 1$. It is worthwhile to note that the family of gW states, for which $E_{A_1A_2:B} = 1$, are given by

$$4 \sum_{i=1}^n a_i^2 = 1 / \sum_{i=n+1}^N a_i^2. \quad (37)$$

The significance of these states will be clear in Sec. III B. For examples of such states, see Appendix D.

Note 3. We point out here that one can also use other entanglement measures, such as the logarithmic negativity or the von Neumann entropy, to demonstrate the above results. With a change in the entanglement measure, the family of gW states providing the bounds [see Eqs. (28) and (37)] remain unchanged, although the functional form of the dependence of $\langle E_{A_1A_2} \rangle$ on $E_{A_1A_2:B}$ [see Eq. (26)] and $\min\{E_{A_1:A_2B}, E_{A_2:A_1B}\}$ [see Eq. (32)] corresponding to the bounds change. In Figs. 2(c) and 2(d), we have demonstrated this pictorially using negativity, logarithmic negativity, and von Neumann entropy as the entanglement measures, although we refrain from writing the equivalent equations corresponding to Eqs. (26) and (32) for these measures to keep the text uncluttered. Note, however, that the bound (3) remains unaltered with a change in entanglement measures.

C. Dicke states

We now consider the class of *symmetric* states that remain invariant under permutation of parties. More specifically, we focus on the Dicke states [58–61] of N qubits, where N_0 qubits are in the ground state $|0\rangle$, and the rest of the $N_1 = N - N_0$ qubits are in the excited state $|1\rangle$. A Dicke state with N_1 excited qubits can be written as

$$|D(N, N_1)\rangle = \frac{1}{\sqrt{\binom{N}{N_1}}} \sum_i \mathcal{P}_i(|0\rangle^{\otimes N-N_1} |1\rangle^{\otimes N_1}), \quad (38)$$

where for a fixed N , $N_1 = 0, 1, 2, \dots, N$. Here, $\{\mathcal{P}_i\}$ is the set of all possible permutations of N_0 (N_1) qubits at the ground (excited) state, such that $N_0 + N_1 = N$. Note that $|D(N, 0)\rangle$ and $|D(N, N)\rangle$ are product states, while $|D_1\rangle$ and $|D_{N-1}\rangle$ are identical to N -qubit W states, or its local unitary equivalents, the results for which can be determined as special cases of the gW states discussed in Sec. II B. Note also that in the case of $n = m < N/2$ ($n = m < (N-1)/2$), where N is even (odd), with m being the size of the subsystem A_1 , symmetry of the Dicke states under qubit permutations suggests that $E_{A_1:A_2B} = E_{A_1A_2:B}$. We focus on the scenario where $n = 1$, and

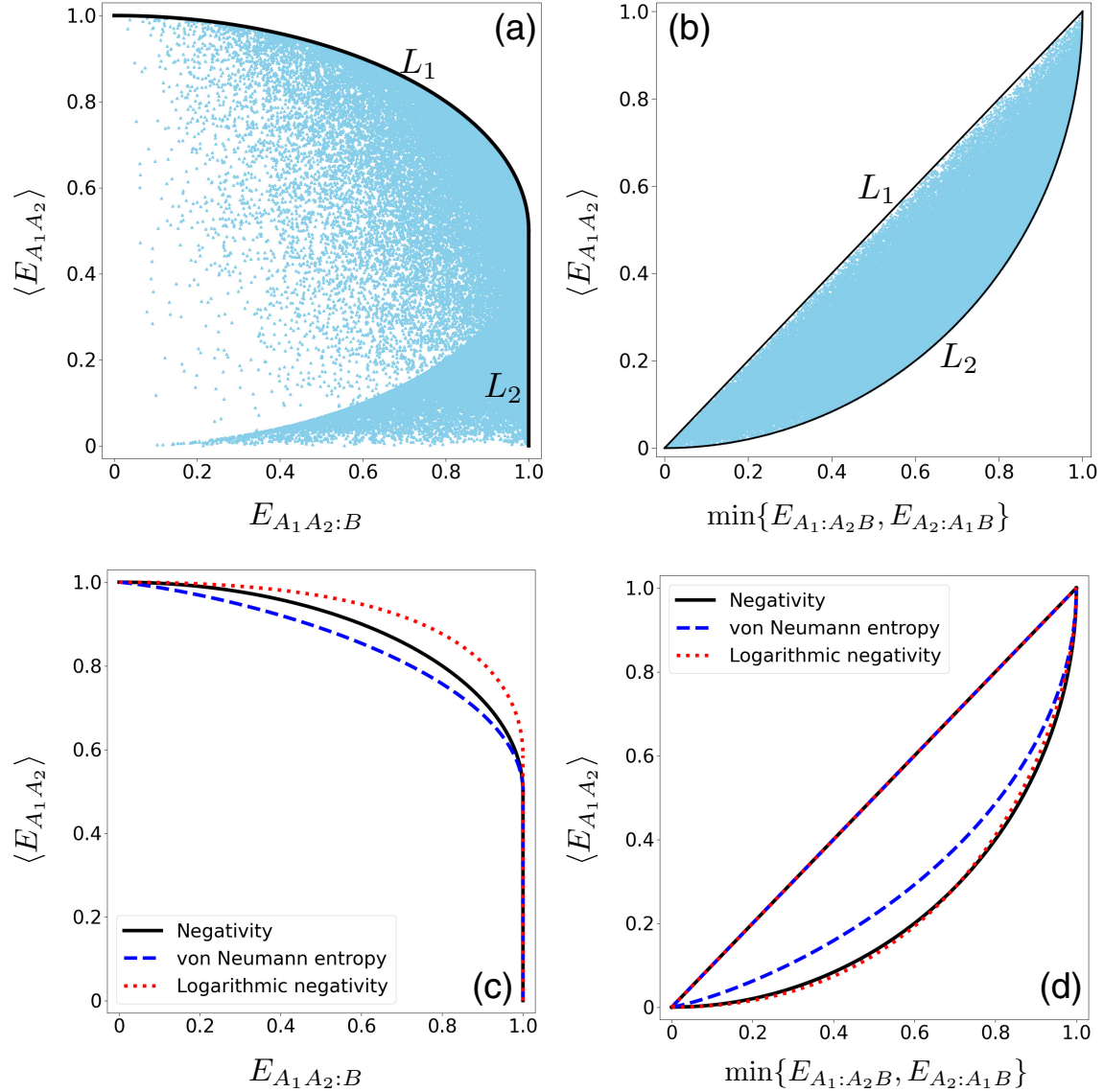


FIG. 2. Generalized W states. Scatter plot of a sample of 10^7 Haar uniformly generated three-qubit gW states on the (a) $(E_{A_1 A_2 : B}, \langle E_{A_1 A_2} \rangle)$ plane and the (b) $(\min\{E_{A_1 : A_2 B}, E_{A_2 : A_1 B}\}, \langle E_{A_1 A_2} \rangle)$ plane, where negativity is used as the entanglement measure. The lines L_1 and L_2 on the $(E_{A_1 A_2 : B}, \langle E_{A_1 A_2} \rangle)$ plane represent, respectively, the family of states following Eq. (26), and $E_{A_1 A_2 : B} = 1$. On the other hand, the lines L_1 and L_2 on the $(\min\{E_{A_1 : A_2 B}, E_{A_2 : A_1 B}\}, \langle E_{A_1 A_2} \rangle)$ plane represent the family of states obeying Eqs. (31) and (32), respectively. The bounds for logarithmic negativity and von Neumann entropy are shown in (c) and (d) along with the same for negativity for comparison (see Sec. II B, Note 3 for a discussion). All quantities plotted are dimensionless, except the entanglement and localizable entanglement computed using von Neumann entropy as the entanglement measure, which are in ebits.

without any loss in generality, measure on qubit 1. Negativity for Dicke states are computable over 1:rest bipartition as [94] (see also Refs. [95,96])

$$E_{A_1 A_2 : B} = \max_{i,j,i \neq j} \frac{1}{\binom{N}{N_1}} \sqrt{\binom{N-1}{N_1-i} \binom{N-1}{N_1-j}}, \quad (39)$$

where B is constituted of one (measured) qubit, and $i, j = 0, 1$. On the other hand, using von Neumann entropy as the entanglement measure [97]:

$$E_{A_1 A_2 : B} = -\frac{N-N_1}{N} \log_2 \frac{N-N_1}{N} - \frac{N_1}{N} \log_2 \frac{N_1}{N}. \quad (40)$$

In the case of $|D(N, N_1)\rangle$, the normalized postmeasured states are given by

$$|D\rangle = \frac{1}{\sqrt{p}} \left[\sqrt{\frac{N-N_1}{N}} \cos \frac{\theta}{2} D(N-1, N_1) + \sqrt{\frac{N_1}{N}} e^{-i\phi} \sin \frac{\theta}{2} D(N-1, N_1-1) \right], \quad (41)$$

$$|D_{\perp}\rangle = \frac{1}{\sqrt{p_{\perp}}} \left[\sqrt{\frac{N-N_1}{N}} \sin \frac{\theta}{2} D(N-1, N_1) - \sqrt{\frac{N_1}{N}} e^{-i\phi} \cos \frac{\theta}{2} D(N-1, N_1-1) \right], \quad (42)$$

with

$$p = \cos^2 \frac{\theta}{2} - \frac{N_1}{N} \cos \theta, \quad (43)$$

$$p_{\perp} = \sin^2 \frac{\theta}{2} + \frac{N_1}{N} \cos \theta. \quad (44)$$

Determination of the general form of any entanglement measure over a bipartition of states of the form $|D\rangle, |D_{\perp}\rangle$, and the subsequent analytical optimization is a difficult task. However, our numerical analysis suggests that the optimization of localizable negativity, in the current situation, always takes place in the σ^z basis. Using this information, $|D\rangle, |D_{\perp}\rangle$ and p, p_{\perp} become

$$\begin{aligned} |D\rangle &= |D(N-1, N_1)\rangle, \\ |D_{\perp}\rangle &= |D(N-1, N_1-1)\rangle, \end{aligned} \quad (45)$$

and

$$p = (N - N_1)/N; \quad p_{\perp} = N_1/N, \quad (46)$$

respectively, resulting in

$$\begin{aligned} \langle E_{A_1 A_2} \rangle &= \max_{i,j,i \neq j} \frac{N - N_1}{N \binom{N-1}{N_1}} \sqrt{\binom{N-2}{N_1-i} \binom{N-2}{N_1-j}} \\ &+ \max_{i,j,i \neq j} \frac{N_1}{N \binom{N-1}{N_1-1}} \sqrt{\binom{N-2}{N_1-1-i} \binom{N-2}{N_1-1-j}}. \end{aligned} \quad (47)$$

when negativity is used as entanglement measure. Using von Neumann entropy instead, one obtains

$$\begin{aligned} \langle E_{A_1 A_2} \rangle &= -M_0[(1 - M_1) \log_2(1 - M_1) \\ &+ M_1 \log_2 M_1] - (1 - M_0)[M_2 \log_2 M_2 \\ &+ (1 - M_2) \log_2(1 - M_2)], \end{aligned} \quad (48)$$

with $M_0 = (N - N_1)/N$, $M_1 = N_1/(N - 1)$ and $M_2 = (N - N_1)/(N - 1)$. It is easy to numerically check that $E_{A_1 A_2 : B} \geq \langle E_{A_1 A_2} \rangle$, which approaches equality as N increases in the case of both negativity and von Neumann entropy. Note also that the variation of $\langle E_{A_1 A_2} \rangle$ with $E_{A_1 A_2 : B}$ is non-monotonic for lower values of N_1 , resulting in a larger difference between $\langle E_{A_1 A_2} \rangle$ and $E_{A_1 A_2 : B}$ at higher N . However, these features disappear as N_1 increases. See Figs. 3(a) and 3(c).

a. Generalized Dicke states. Using the Dicke states, one can define an N -qubit permutation-symmetric state in the form of a gD state [42], as

$$|D(N)\rangle = \sum_{N_1=0}^N a_{N_1} |D(N, N_1)\rangle, \quad (49)$$

where $a_{N_1} \in \mathbb{C}$, and $\sum_{N_1=0}^N |a_{N_1}|^2 = 1$. Due to a large number of state parameters, analytical calculation is difficult for gD states. However, as in the case of the Dicke states, the permutation symmetry can be used here also to have $E_{A_1 : A_2 B} = E_{A_1 A_2 : B}$ in the case of $n = m < N/2$ ($n = m < (N - 1)/2$) for even (odd) N . This implies that it is sufficient to look into the relation between $\langle E_{A_1 A_2} \rangle$ and $\min\{E_{A_1 : A_2 B}, E_{A_2 : A_1 B}\}$, which is given by (3). Moreover, our numerical results suggest that

$\min\{E_{A_1 : A_2 B}, E_{A_2 : A_1 B}\} = E_{A_1 : A_2 B}$ for all Haar uniformly generated gD states, which leads to the upper bound of $\langle E_{A_1 A_2} \rangle$ as $\langle E_{A_1 A_2} \rangle \leq E_{A_1 A_2 : B}$ [see Figs. 3(b) and 3(d)]. It is clear from the scatter diagrams that as N increases, the difference between $E_{A_1 A_2 : B}$ and $\langle E_{A_1 A_2} \rangle$ decreases, and considerably larger fraction of states are found to obey $\langle E_{A_1 A_2} \rangle = E_{A_1 A_2 : B}$ in the situation where each of the subsystems B and A_1 holds only one qubit.

D. Arbitrary multiqubit pure states

In this section, we investigate the question posed in Sec. I for arbitrary states of systems with arbitrary number of qubits.

a. Three-qubit systems. While analytical calculation of the relevant quantities is difficult for a large number of qubits, in relation to Proposition II, some analytical results can be derived for the three-qubit systems ($N = 3$) with $n = m = 1$. Note that the three-qubit gW states are a subset of the three-qubit W class states, which, together with the three-qubit GHZ class states, form the complete set of three-qubit pure states [56]. We explore whether the bound in Proposition II also applies to the three-qubit W class states given by [56]

$$|\psi_W\rangle = a_0|000\rangle + a_1|100\rangle + a_2|010\rangle + a_3|001\rangle, \quad (50)$$

where $\sum_{i=0}^3 |a_i|^2 = 1$ and $a_i \in \mathbb{C}$, $i = 0, 1, 2, 3$. For ease of discussion, we consider qubits 1, 2, and 3 to be subsystems B , A_1 , and A_2 , respectively. Also, we first consider the subclass of the W -class states with real coefficients only, i.e., $a_i \in \mathbb{R}$, $i = 0, 1, 2, 3$, and numerically verify that the negativity over different bipartitions of the three-qubit W -class states are given by

$$E_{1:23} = 2|a_1 \sqrt{a_2^2 + a_3^2}|, \quad (51)$$

$$E_{2:13} = 2|a_2 \sqrt{a_1^2 + a_3^2}|, \quad (52)$$

$$E_{3:12} = 2|a_3 \sqrt{a_1^2 + a_2^2}|. \quad (53)$$

Further, performing local projection measurements in the basis $\{|b_0\rangle, |b_1\rangle\}$ on qubit 1, one obtains the postmeasured states on qubits 2 and 3 to be in the same form as in Eq. (22), with f_0^k and f^k ($k = 0, 1$) given in Appendix B. Similar to the three-qubit gW states, negativity of the postmeasured states are independent of the measurement basis and are given by $2|a_2||a_3|$. This leads to

$$\langle E_{23} \rangle = 2|a_2||a_3|. \quad (54)$$

We are now in a position to present the following proposition for the W class states of three qubits.

Proposition IV. In the space $(E_{1:23}, \langle E_{23} \rangle)$, the localizable entanglement $\langle E_{23} \rangle$ of a three-qubit normalized W -class state with real coefficients is upper bounded by the line

$$\langle E_{23} \rangle = \frac{1}{2}(1 + \sqrt{1 - E_{1:23}^2}), \quad (55)$$

where $E_{1:23}$ is the bipartite entanglement over the bipartition $1 : 23$ in the state prior to measurement on qubit 1.

Proof. Similar to the case of the gW states, we can write $\langle E_{23} \rangle^2$ as

$$\langle E_{23} \rangle^2 = 4a_2^2(1 - a_0^2 - a_1^2 - a_2^2). \quad (56)$$

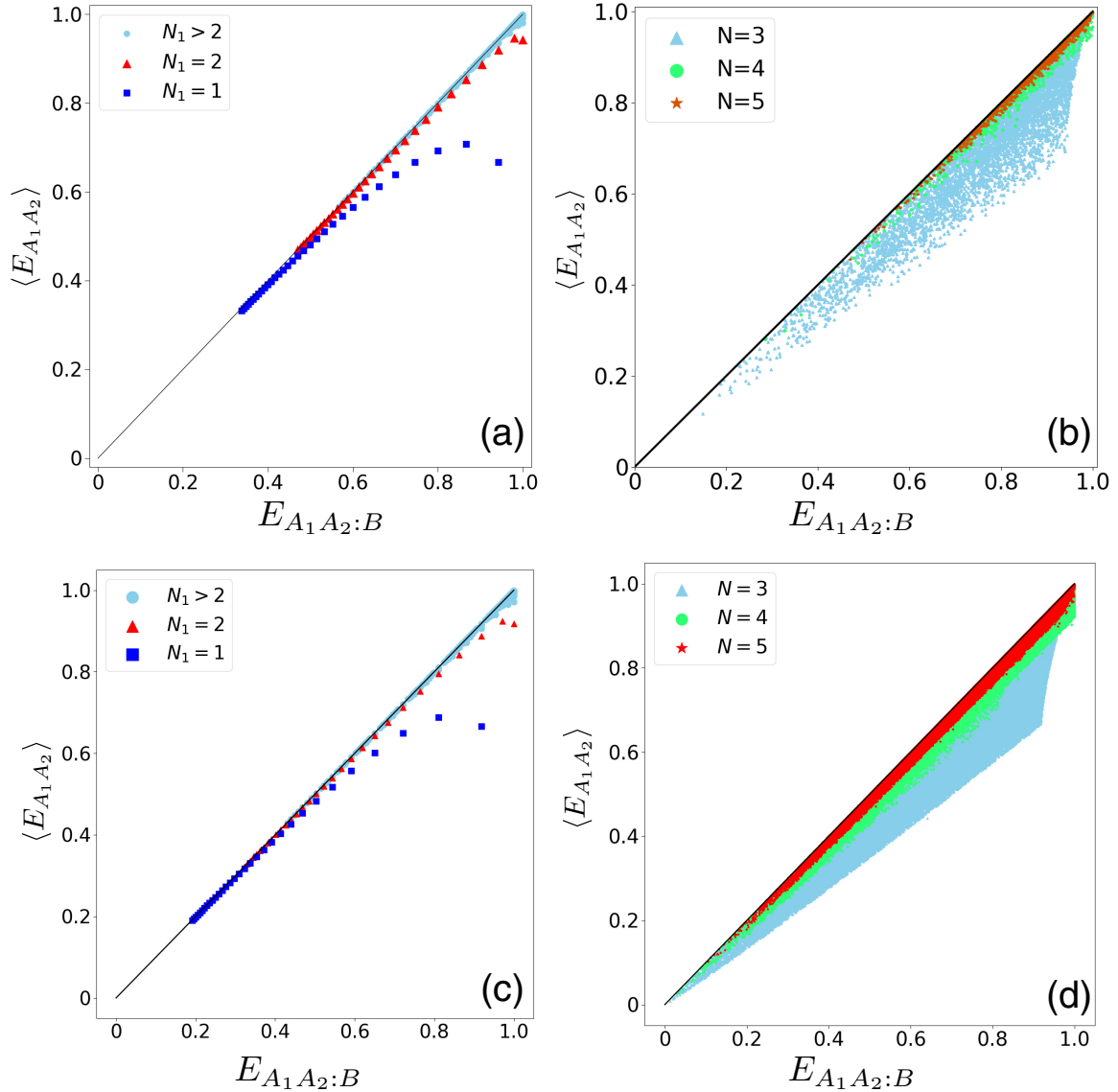


FIG. 3. Dicke states. (a), (c) Scatter plots of $|D(N, N_1)\rangle$ for $N \leq 35$ on the $(E_{A_1 A_2 : B}, \langle E_{A_1 A_2} \rangle)$ plane, with all possible values of $N_1 = 1, \dots, N - 1$, using (a) negativity and (c) von Neumann entropy as entanglement measures. (b), (d) Scatter plot of Haar uniformly generated gD states of $N = 3, N = 4$, and $N = 5$ qubits on the $(E_{A_1 A_2 : B}, \langle E_{A_1 A_2} \rangle)$ plane, where each of the subsystems B and A_1 are constituted of one qubit only. For each value of N , a sample of 10^5 states are used. The chosen entanglement measures are (b) negativity and (d) von Neumann entropy. All quantities plotted are dimensionless, except the entanglement and localizable entanglement computed using von Neumann entropy as the entanglement measure, which are in ebits.

For a fixed value of $a_0^2 + a_1^2 = a^2$, the maximum of $\langle E_{23} \rangle^2$, and therefore of $\langle E_{23} \rangle$, occurs at $a_2^2 = (1 - a^2)/2$, the maximum value of $\langle E_{23} \rangle$ being $(1 - a^2)$. Also, $E_{1:23} = 2|a_1 \sqrt{1 - a^2}|$. Note that the maximum value of $\langle E_{23} \rangle$ as well as $E_{1:23}$ have two free parameters, a_0 and a_1 , constrained by $a_0^2 + a_1^2$ being a constant, a^2 . Eliminating a_1 from $\langle E_{23} \rangle$ and $E_{1:23}$, followed by solving for $\langle E_{23} \rangle$, leads to

$$\langle E_{23} \rangle = \frac{1}{2} \left[(1 - a_0^2) + \sqrt{(1 - a_0^2)^2 - E_{1:23}^2} \right], \quad (57)$$

where $0 \leq a_0^2 \leq a^2$. Further maximization with respect to a_0 implies $a_0 = 0$, leading to Eq. (55). ■

Similar to the three-qubit gW states, the following corollaries originate from Proposition IV.

Corollary IV.1. The family of W class states with real coefficients that satisfy Eq. (55) are given by

$$a_2^2 = a_3^2 = (1 - a_1^2)/2. \quad (58)$$

Proof. The proof of this corollary follows from the maximization condition of $\langle E_{23} \rangle$, and the normalization of the W-class state. ■

Corollary IV.2. For the family of W-class states given by Eq. (58), $E_{2:13} = E_{3:12}$.

Proof. The proof of this corollary follows from identifying the states satisfying Eq. (58) as the three-qubit gW states, and from the proof of Corollary II.2. ■

Proposition V. In $(\min\{E_{2:13}, E_{3:12}\}, \langle E_{23} \rangle)$ space, the localizable entanglement $\langle E_{23} \rangle$ of a three-qubit normalized W-class

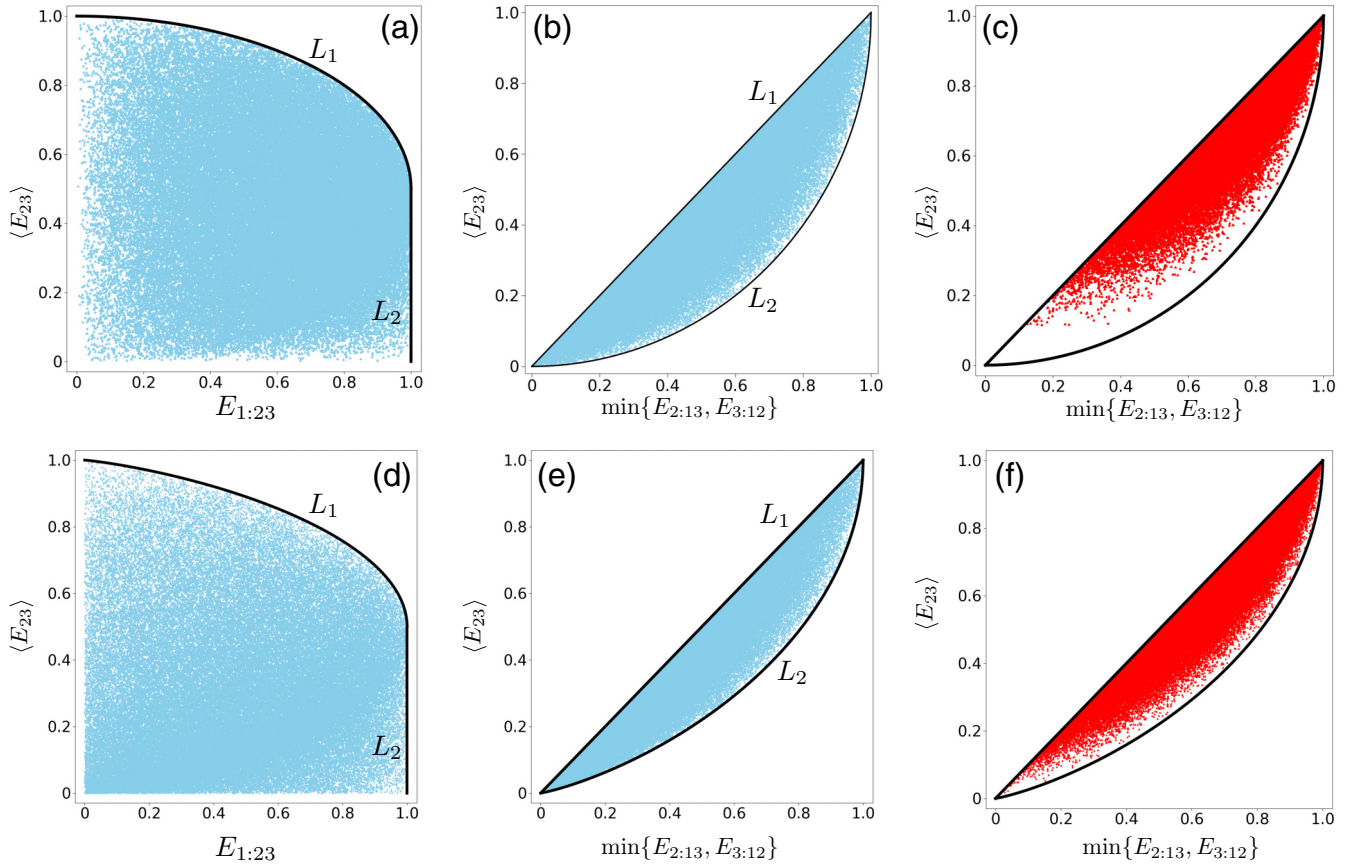


FIG. 4. GHZ and W -class states. Scatter plot of a sample of 10^7 Haar-uniformly generated three-qubit W -class states on the (a) $(E_{1:23}, \langle E_{23} \rangle)$ and (b) $(\min\{E_{2:13}, E_{3:12}\}, \langle E_{23} \rangle)$ plane. The lines L_1 and L_2 bounding the states correspond to Eq. (55) and $E_{1:23} = 1$, respectively. (c) A sample of 10^7 Haar uniformly generated GHZ-class states are also found to be bound by the same upper and lower bounds as proposed in Proposition III. In (a)–(c), negativity is used as entanglement measure, while the corresponding figures for von Neumann entropy are given in (d)–(f). All quantities plotted are dimensionless, except the entanglement and localizable entanglement computed using von Neumann entropy as the entanglement measure, which are in ebits.

state with real coefficients is upper-bounded by the line

$$\langle E_{23} \rangle = \min\{E_{2:13}, E_{3:12}\}, \quad (59)$$

and lower bounded by the line

$$\langle E_{23} \rangle^2 - 2\langle E_{23} \rangle + (\min\{E_{2:13}, E_{3:12}\})^2 = 0, \quad (60)$$

where $E_{2:13}$ ($E_{3:12}$) is the bipartite entanglement over the bipartition 2 : 13 (3 : 12) in the state prior to measurement on the qubit 1.

Proof. Similar to the proof of Proposition III, the upper bound follows from the monotonicity of E [see Eq. (3)]. To prove the lower bound, we start by assuming $E_{2:13} \geq E_{3:12}$ and $\min\{E_{2:13}, E_{3:12}\} = E_{3:12}$, which, by virtue of Eqs. (52) and (53), implies $a_2^2 \geq a_3^2$. For a fixed a_3 and a_0 , $\langle E_{23} \rangle$ is minimum if a_2 is minimum, leading to $a_2 = a_3$, and subsequently $\langle E_{23} \rangle \geq 2a_3^2$. On the other hand, exploiting normalization of the W -class state, $E_{3:12} = 2|a_3\sqrt{1 - a_0^2 - a_3^2}|$. Eliminating a_3 from $E_{3:12}$ and the minimum of $\langle E_{23} \rangle$, we obtain

$$\langle E_{23} \rangle^2 + E_{3:12}^2 - 2\langle E_{23} \rangle(1 - a_0^2) = 0. \quad (61)$$

Similar to Proposition V, it can be shown that $\langle E_{23} \rangle$ attains a minimum for $a_0 = 0$, leading to Eq. (60). ■

Note 4. Similar to the case of N -qubit gW states, in this case also, we numerically verify that the Propositions IV and

V remain valid in the case of generic three-qubit states from W class with complex coefficients. The bounds in the case of three-qubit W class states are demonstrated in Figs. 4(a) and 4(b).

Note 5. We also investigate the three-qubit GHZ class states, given by

$$|\psi_{\text{GHZ}}\rangle = \sum_{i=0}^7 c_i |\phi_i\rangle, \quad (62)$$

with $c_i \in \mathbb{C}$ and $\{|\phi_i\rangle; i = 0, 1, \dots, 7\}$ being the standard product basis in the Hilbert space of three qubits. While analytical investigation is difficult due to a large number of parameters involved in these states, our numerical analysis does not provide any evidence of the existence of an upper bound of $\langle E_{23} \rangle$ on the $(E_{1:23}, \langle E_{23} \rangle)$ plane. However, our investigation involving a sample of 10^7 Haar uniformly generated GHZ-class states did not find any example that violates the lower bound proposed in Proposition V [see Fig. 4(c) for a demonstration]. While this does not analytically prove the validity of the lower bound, this implies that Proposition IV has the potential to distinguish between the three-qubit W class states from the GHZ class states.

TABLE I. Variations of the fraction of Haar uniformly generated three-, four-, and five-qubit states for which $\delta_1 > 0$, as a function of the noise parameter q , which assumes five values, $q = 0.0, 0.1, 0.2, 0.3$, and 0.4 , from left to right along the row for a specific combination of N , n , and m , in the case of the Markovian phase-flip noise, where negativity is used as entanglement measure. In all cases, we have kept $n = 1$, where n and m being the sizes of B and A_1 respectively. For the three-qubit system, only GHZ class states are considered. For each case, the percentages are determined from a sample size of 10^5 Haar uniformly generated states.

N	n	m	Fraction of states (in %) with $\delta_1 > 0$				
			$q = 0.0$	$q = 0.1$	$q = 0.2$	$q = 0.3$	$q = 0.4$
3	1	1	23.343%	23.608%	23.097%	21.530%	18.890%
4	1	1	38.704%	20.461%	15.757%	15.514%	15.336%
5	1	1	44.920%	14.213%	12.942%	10.531%	07.487%
5	1	2	100.00%	100.00%	100.00%	100.00%	93.402%

b. Larger systems. To study the correlation between localizable entanglement $\langle E_{A_1 A_2} \rangle$ and the bipartite entanglement lost due to the measurement, namely, $E_{A_1 A_2 : B}$, $E_{A_1 : A_2 B}$, and $E_{A_2 : A_1 B}$ in the case of pure states on N qubits, we look into how the states are distributed on the $(E_{A_1 A_2 : B}, \langle E_{A_1 A_2} \rangle)$ and the $(\min\{E_{A_1 : A_2 B}, E_{A_2 : A_1 B}\}, \langle E_{A_1 A_2} \rangle)$ spaces. To investigate this, we define the following:

$$\delta_1 = \langle E_{A_1 A_2} \rangle - E_{AB}, \quad (63)$$

$$\delta_2 = \langle E_{A_1 A_2} \rangle - \min\{E_{A_1 B : A_2}, E_{A_2 B : A_1}\}. \quad (64)$$

Note that $\delta_1 \geq 0$ ($\delta_2 \geq 0$) implies $\langle E_{A_1 A_2} \rangle \geq E_{A_1 A_2 : B}$ ($\langle E_{A_1 A_2} \rangle \geq \min\{E_{A_1 B : A_2}, E_{A_2 B : A_1}\}$), which is representative of a situation where one can, on average, localize at least $E_{A_1 A_2 : B}$ ($\min\{E_{A_2 : A_1 B}, E_{A_1 : A_2 B}\}$) amount of entanglement via local projection measurements on the qubits in B . The percentages of N -qubit states for which $\delta_1 > 0$ are included in Table I for different combinations of N and m , keeping $n = 1$, where in each case, a sample of 10^5 Haar uniformly generated pure states are considered. Clearly, the percentage of states for which $\delta_1 > 0$ increases overall with the increase in the number of qubits, implying that the number of states for which $\langle E_{A_1 A_2} \rangle > E_{A_1 A_2 : B}$ are more for larger systems. However, the percentage of states for which $\delta_1 = 0$, up to our numerical accuracy, is negligibly small for all cases of (N, n, m) . On the other hand, as expected, $\delta_2 > 0$ does not occur for any multiqubit pure states, as it would imply a violation of (3). Moreover, for a very small fraction of states, $\delta_2 = 0$. This fraction overall increases with an increase in the number of qubits in the system.

Note 6. We point out here that the analysis presented in Sec. II D can also be carried out using entanglement measures other than negativity, where no qualitative results are changed except Eqs. (57) and (60). While we refrain from writing the corresponding equivalent equations, we pictorially demonstrate this in Figs. 4(d)–4(f) using von Neumann entropy. Similar features are also found for logarithmic negativity. Note also that the data included in Table I are specific to the choice of negativity as an entanglement measure.

III. QUANTUM STATES UNDER PHASE-FLIP NOISE

It is now logical to ask whether and how the results reported in Sec. II are modified if the multiqubit system is subjected to noise [62]. In this paper, we consider a situation where qubits of the multiqubit system are sent through

independent phase-flip channels [62,63]. These phase-flip channels can be either Markovian [64] or non-Markovian [65–67]. Using the Kraus operator representation, the evolution of the quantum state $\rho_0 = |\psi\rangle\langle\psi|$ under these phase-flip channels is given by

$$\rho = \sum_{\alpha} K_{\alpha} \rho_0 K_{\alpha}^{\dagger}, \quad (65)$$

such that $\sum_{\alpha} K_{\alpha}^{\dagger} K_{\alpha} = I$, I being the identity operator in the Hilbert space of the multiqubit system, and Kraus operators $\{K_{\alpha}\}$, takes the form $K_{\alpha} = \sqrt{p_{\alpha}} K'_{\alpha}$ with

$$K'_{\alpha} = \bigotimes_{i=1}^N K'_{\alpha_i}; \quad p_{\alpha} = \prod_{i=1}^N p_{\alpha_i}. \quad (66)$$

Here, the index $\alpha \equiv \alpha_1 \alpha_2 \cdots \alpha_N$ is interpreted as a multi-index, $\sum_{\alpha_i} p_{\alpha_i} = 1$, and K'_{α_i} are the single-qubit Kraus operators, the form of which depends on the type of noise under consideration. In the case of the phase-flip noise, $\alpha_i \in \{0, 1\}$, $K'_{\alpha_i=0} = I_i$, and $K'_{\alpha_i=1} = \sigma_i^z$, with

$$p_{\alpha_i=0} = 1 - \frac{q}{2}, \quad p_{\alpha_i=1} = \frac{q}{2} \quad (67)$$

in the Markovian case [64], and

$$p_{\alpha_i=0} = \left(1 - \frac{q}{2}\right) \left(1 - \frac{\alpha q}{2}\right),$$

$$p_{\alpha_i=1} = \left[1 + \alpha \left(1 - \frac{q}{2}\right)\right] \frac{q}{2} \quad (68)$$

in the non-Markovian case [65–67]. Here, q is the noise strength ($0 \leq q \leq 1$) and α is the non-Markovianity parameter ($0 \leq \alpha \leq 1$). For ease of discussion, from now onward, we denote entanglement in the noiseless scenario with a superscript 0. For example, $\langle E_{A_1 A_2} \rangle^0$ and E_{AB}^0 denote the localizable entanglement over subsystem A and the bipartite entanglement overbipartition $A : B$ of the system in the case of ρ_0 . Also, in this section, we use negativity as an entanglement measure to demonstrate all our results.

A. Generalized GHZ states

We start our discussions with the N -qubit gGHZ state subjected to phase-flip noise on all qubits. In this situation, we prove the following proposition.

Proposition VI. For any tripartition $A_1 : A_2 : B$ of an N -qubit gGHZ state under uncorrelated phase-flip channel on all

qubits,

$$\langle E_{A_1 A_2} \rangle = E_{A_1 A_2 : B} = E_{A_1 : A_2 B} = E_{A_2 : A_1 B}, \quad (69)$$

irrespective of whether the noise is Markovian or non-Markovian.

Proof. The N -qubit gGHZ state, under the Markovian phase-flip noise on all qubits, takes the form

$$\rho = (|a_0|^2(|0\rangle\langle 0|)^{\otimes N} + |a_1|^2(|1\rangle\langle 1|)^{\otimes N}) + (1 - q)^N (a_0 a_1^* (|0\rangle\langle 1|)^{\otimes N} + a_0^* a_1 (|1\rangle\langle 0|)^{\otimes N}). \quad (70)$$

Partial transposition of ρ with respect to the subsystems B leads to

$$\rho^{T_B} = (|a_0|^2(|0\rangle\langle 0|)^{\otimes N} + |a_1|^2(|1\rangle\langle 1|)^{\otimes N}) + (1 - q)^N a_0 a_1^* (|0\rangle\langle 1|)^{\otimes N-n} (|1\rangle\langle 0|)^{\otimes n} + (1 - q)^N a_0^* a_1 (|1\rangle\langle 0|)^{\otimes N-n} (|0\rangle\langle 1|)^{\otimes n}, \quad (71)$$

with nonzero eigenvalues $|a_0|^2, |a_1|^2, \pm(1 - q)^N |a_0| |a_1|$. Therefore, the entanglement between partition A and partition B , as quantified by negativity [81–85], is given by

$$E_{A_1 A_2 : B} = 2(1 - q)^N |a_0| \sqrt{1 - |a_0|^2} = (1 - q)^N E_{A_1 A_2 : B}^0. \quad (72)$$

To calculate the localizable entanglement over subsystem A with bipartition $A_1 : A_2$, we proceed as in the case of Proposition I, and write the postmeasured states on A as

$$\tilde{\rho}_A^k = \text{Tr}_B[(M^k \rho M^{k\dagger})/p_k], \quad (73)$$

which, written explicitly, takes the form

$$\tilde{\rho}_A^k = \frac{1}{p_k} [\{|a_0|^2 |f_0^k|^2 (|0\rangle\langle 0|)^{\otimes N-n} + |a_1|^2 |f_1^k|^2 (|1\rangle\langle 1|)^{\otimes N-n}\} + (1 - q)^N \{a_0 a_1^* f_0^k f_1^{k*} (|0\rangle\langle 1|)^{\otimes N-n} + a_0^* a_1 f_1^k f_0^{k*} (|1\rangle\langle 0|)^{\otimes N-n}\}], \quad (74)$$

with

$$p_k = (|a_0|^2 |f_0^k|^2 + |a_1|^2 |f_1^k|^2). \quad (75)$$

Partial transposition of $\tilde{\rho}_A^k$ over any bipartition $A_1 : A_2$, and subsequent calculation of negativity followed by the optimization of average negativity over $A_1 : A_2$ yields

$$\langle E_{A_1 : A_2} \rangle = 2(1 - q)^N |a_0| \sqrt{1 - |a_0|^2} \left[\max_{k=0}^{2^n - 1} \sum_{k=0} |f_0^k| |f_1^k| \right], \quad (76)$$

as in Eq. (14). The maximization is similar to that shown in the proof of Proposition I, leading to

$$\langle E_{A_1 : A_2} \rangle = (1 - q)^N \langle E_{A_1 A_2} \rangle^0 = E_{A_1 A_2 : B}. \quad (77)$$

Also, from the symmetry of ρ , $E_{A_1 A_2 : B} = E_{A_1 : A_2 B} = E_{A_2 : A_1 B}$, leading to Eq. (69).

The same line of calculations would follow for the non-Markovian phase-flip channel, leading to

$$E_{A_1 A_2 : B} = |1 - f(q, \alpha)|^N E_{A_1 A_2 : B}^0, \quad \langle E_{A_1 A_2} \rangle = |1 - f(q, \alpha)|^N \langle E_{A_1 A_2} \rangle^0, \quad (78)$$

with

$$f(q, \alpha) = q \left\{ 1 + \alpha \left(1 - \frac{q}{2} \right) \right\}, \quad (79)$$

which implies $\langle E_{A_1 A_2} \rangle = E_{A_1 A_2 : B}$. A similar proof follows for $E_{A_1 : A_2 B}$, and $E_{A_2 : A_1 B}$ also, resulting in Eq. (69) for the non-Markovian phase-flip channel. Hence the proof. ■

Note 7. A comparative discussion on the variation of entanglement with q in the cases of the Markovian and the non-Markovian phase-flip channels is in order here. Note that in the former case, entanglement decays monotonically with q , as indicated from the $(1 - q)^N$ dependence, while the decay fastens exponentially with increasing number of qubits. It also indicates that entanglement vanishes asymptotically with increasing q , attaining zero value only at $q = 1$. Similar features are also present in the case of the non-Markovian channel, except one where in contrast to entanglement vanishing only at $q = 1$ in the former case, entanglement vanishes at a finite critical q in the latter, given by

$$q_c = \frac{1}{\alpha} (1 + \alpha - \sqrt{1 + \alpha^2}). \quad (80)$$

For $q > q_c$, entanglement revives again. Note that q_c is a monotonically decreasing function of α , which, in the limit $\alpha \rightarrow 0$ (the Markovian limit), goes to 1.

B. Generalized W states

We now focus on the N -qubit gW states under the phase-flip noise on all qubits. Analytical investigation of $\langle E_{A_1 A_2} \rangle$ as well as bipartite entanglement over the unmeasured state in such cases is difficult due to the increasing number of state as well as optimization parameters. However, our numerical investigation suggests that irrespective of the tripartition $A_1 : A_2 : B$ of the N -qubit system, the optimization of $\langle E_{A_1 A_2} \rangle$ always takes place via σ^z measurement on all qubits $i \in B$. This result can be utilized to determine the dependence of $\langle E_{A_1 A_2} \rangle$ and $E_{A_1 A_2 : B}$ on the noise strength q , and extend the Propositions II and III, as follows.

a. Markovian phase-flip channels. In the case of the Markovian phase-flip channels, we obtain⁴

$$\langle E_{A_1 A_2} \rangle = (1 - q)^2 \langle E_{A_1 A_2} \rangle^0, \quad (81)$$

$$E_{A_1 A_2 : B} = (1 - q)^2 E_{A_1 A_2 : B}^0, \quad (82)$$

Given these results, we present the following proposition.

Proposition VII. In the space $(E_{A_1 A_2 : B}, \langle E_{A_1 A_2} \rangle)$, the localizable entanglement $\langle E_{A_1 A_2} \rangle$ of an N -qubit normalized gW

⁴These expressions are determined for systems of small sizes, and are verified numerically for larger systems with different combinations of (N, n, m) .

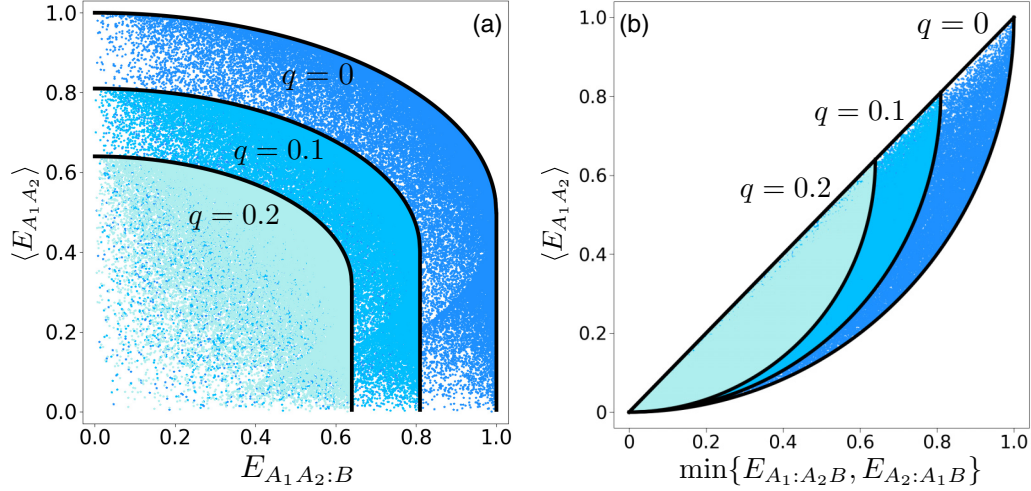


FIG. 5. Generalized W states under Markovian phase-flip channels. Modification of boundaries of gW states proposed in Propositions II and III on the (a) $(E_{A_1 A_2 : B}, \langle E_{A_1 A_2} \rangle)$ and (b) $(\min\{E_{A_1 : A_2 B}, E_{A_2 : A_1 B}\}, \langle E_{A_1 A_2} \rangle)$ plane due to Markovian phase-flip noise of noise strength $q = 0, 0.1, 0.2$ (see also Fig. 2), using negativity as the entanglement measure. The modified boundaries are given in Propositions VI and VII. The trivial boundaries corresponding to zero entanglement lines are not shown. All quantities plotted in all figures are dimensionless.

state subjected to Markovian phase-flip channels of the same strength, q , on all qubits is bounded by the lines

$$\langle E_{A_1 A_2} \rangle = \frac{1}{2} \left[(1-q)^2 + \sqrt{(1-q)^4 - E_{A_1 A_2 : B}^2} \right], \quad (83)$$

and

$$E_{A_1 A_2 : B} = (1-q)^2, \quad (84)$$

where $E_{A_1 A_2 : B}$ is the bipartite entanglement over the bipartition $A_1 A_2 : B$ in the state prior to measurement on all the qubits in B .

Note 8. It is worthwhile to note that the line given in Eq. (84) corresponds to the family of states, described by Eq. (37), subjected to the single-qubit phase-flip channels on all qubits.

Note 9. Proposition VI implies that the area on the $(E_{A_1 A_2 : B}, \langle E_{A_1 A_2} \rangle)$ plane confining the noisy gW states shrinks with increasing noise strength q , and vanishes at $q = 1$. This is demonstrated in Fig. 5(a).

Noting that $E_{A_1 : A_2 B}$ and $E_{A_2 : A_1 B}$ also have a similar dependence on q as $E_{A_1 A_2 : B}$, Proposition III can be extended to the case of gW states under phase-flip noise, as follows.

Proposition VIII. In $(\min\{E_{A_1 : A_2 B}, E_{A_2 : A_1 B}\}, \langle E_{A_1 A_2} \rangle)$ space, the localizable entanglement $\langle E_{A_1 A_2} \rangle$ of an N -qubit normalized gW state subjected to the phase-flip channel of strength q on all qubits is upper-bounded by the line

$$\langle E_{A_1 A_2} \rangle = \min\{E_{A_1 : A_2 B}, E_{A_2 : A_1 B}\}, \quad (85)$$

and lower bounded by the line

$$\langle E_{A_1 A_2} \rangle^2 - 2(1-q)^2 \langle E_{A_1 A_2} \rangle + (\min\{E_{A_1 : A_2 B}, E_{A_2 : A_1 B}\})^2 = 0, \quad (86)$$

where $E_{A_1 : A_2 B}$ ($E_{A_2 : A_1 B}$) is the entanglement over the bipartition $A_1 : A_2 B$ ($A_2 : A_1 B$) in the state prior to measurement on all the qubits in B .

b. Non-Markovian phase-flip channels. A similar approach can also be taken in the case of the non-Markovian

channels, where entanglement has the following dependence on q and α :

$$\langle E_{A_1 A_2} \rangle = |1 - f(q, \alpha)|^2 \langle E_{A_1 A_2} \rangle^0, \quad (87)$$

$$E_{A_1 A_2 : B} = |1 - f(q, \alpha)|^2 E_{A_1 A_2 : B}^0, \quad (88)$$

$$E_{A_1 : A_2 B} = |1 - f(q, \alpha)|^2 E_{A_1 : A_2 B}^0, \quad (89)$$

$$E_{A_2 : A_1 B} = |1 - f(q, \alpha)|^2 E_{A_2 : A_1 B}^0, \quad (90)$$

with $f(q, \alpha)$ given in Eq. (79). Using these, one can straightforwardly obtain the results on the bounds on the gW states when subjected to non-Markovian phase-flip channels, by replacing the $(1-q)^2$ factors with $|1 - f(q, \alpha)|^2$. To keep the text uncluttered, we refrain from writing these Propositions explicitly.

Similar to the Markovian case, for a fixed value of α , the area on the $E_{A_1 A_2 : B} - \langle E_{A_1 A_2} \rangle$ plane confining the noisy gW states shrinks with increasing q in the case of the non-Markovian phase flip channel also. However, in contrast to the Markovian case, the area vanishes at a critical noise strength q_c , given in Eq. (80), and then revives again for $q > q_c$ (see Fig. 6 for a demonstration). It is worthwhile to note that the decay of entanglement in the case of the gW states under Markovian and non-Markovian phase-flip channels is independent of the number of qubits in the system, as opposed to the case of the gGHZ states, where the dependence is exponential in N .

C. Numerical results

The complexity of the states obtained via applying single-qubit phase-flip noise to all qubits of a multiqubit states prevents analytical investigation into the relation between the localizable and the destroyed entanglement in most cases. In this subsection, we discuss the numerical results obtained for the mixed states generated via subjecting three-qubit W -class states, N -qubit Dicke and gD states, and arbitrary N -qubit

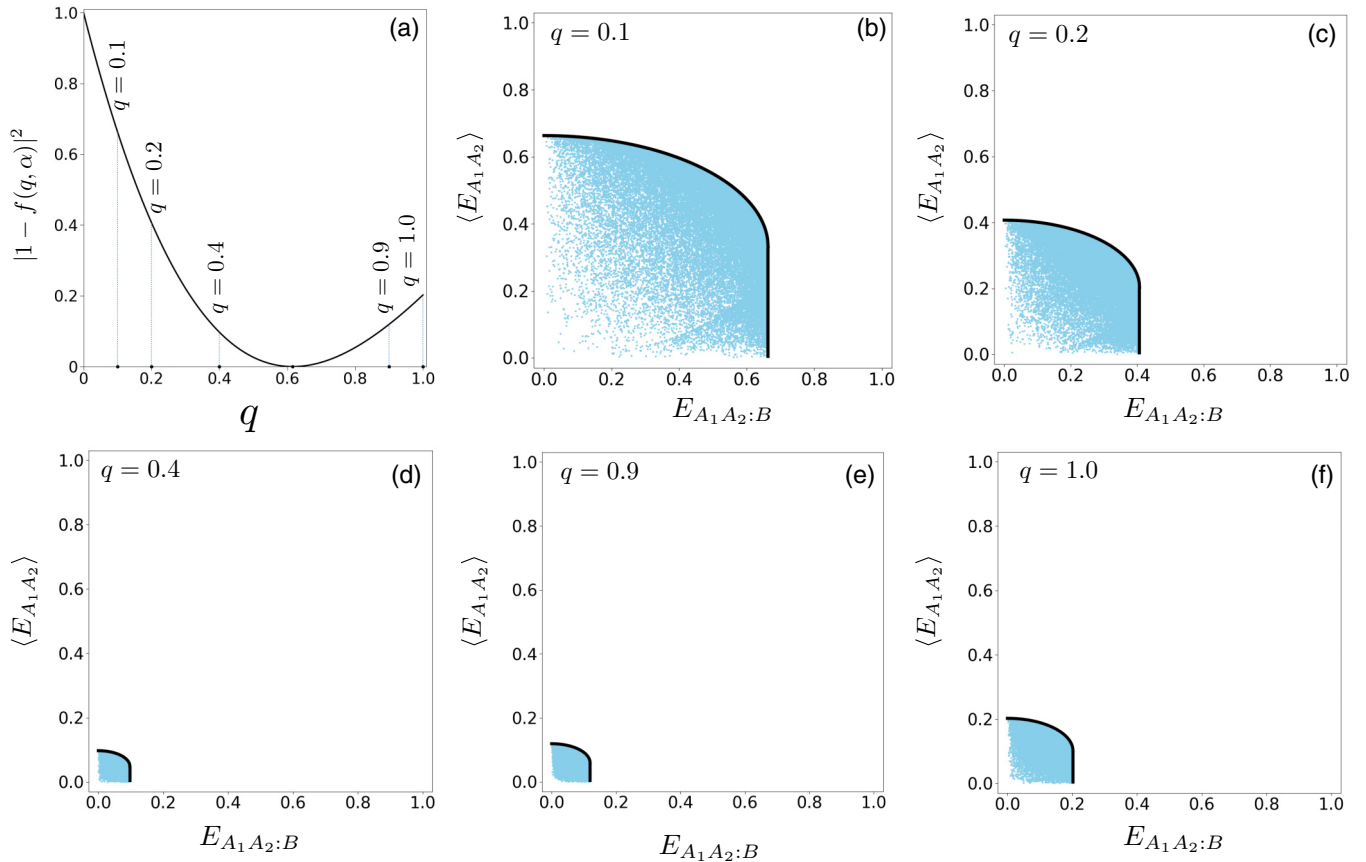


FIG. 6. Generalized W states under non-Markovian phase-flip noise. (a) The variation of $|1 - f(q, \alpha)|^2$ as a function of q for $\alpha = 0.9$, demonstrating the variation of entanglement with q [see Eqs. (87)–(90)], which exhibits monotonic decay followed by a vanishing at q_c [Eq. (80)] and a subsequent revival for $q > q_c$, where negativity is used as entanglement measure. In the entire range $0 \leq q \leq 1$, five values of noise strengths, namely, (b) $q = 0.1$, (c) $q = 0.2$, (d) $q = 0.4$, (e) $q = 0.9$, and (f) $q = 1.0$ are chosen, and the modification of the boundaries on the four-qubit gW states, as given in Proposition II, with varying q is demonstrated. The region accessible by the gW states on the $(E_{A_1 A_2 : B}, \langle E_{A_1 A_2} \rangle)$ decreases at first, vanishes at $q = q_c$, and then revives again. All quantities plotted in all figures are dimensionless.

pure states to Markovian and non-Markovian phase-flip channels.

a. Three-qubit states. Our numerical investigation of the three-qubit W -class states subjected to Markovian as well as non-Markovian phase-flip channels indicate that the variations of the localizable entanglement $\langle E_{23} \rangle$ as well as the bipartite entanglement lost during measurement, namely, $E_{1:23}$, $E_{2:13}$, and $E_{3:12}$, are identical to that described in Eqs. (81) and (82) (Markovian) and Eqs. (87)–(90) (non-Markovian). This implies that the mixed states obtained from the three-qubit W -class states, for a specific noise strength q , are bounded in a similar way as described for the gW states under phase-flip noise. On the other hand, while a similar numerical analysis is difficult for the GHZ class states due to the increased number of parameters, we observe that similar to the pure GHZ-class states discussed in Note 4 [see also Fig. 4(c)], the bounds proposed in Eqs. (85) and (86) hold also for three-qubit GHZ-class states subjected to the Markovian phase-flip noise channels.

b. Dicke states and generalized Dicke states under noise. We also numerically investigate the N -qubit Dicke and gD states subjected to Markovian and non-Markovian phase-flip channels. Figures 7(a) and 7(b) depict the scatter plots of the Dicke states up to $N = 8$, and $N_1 = 1, 2$, where Markovian

and non-Markovian phase-flip channel is applied to all qubits. It is clear from the figures that similar to the case of the Pure Dicke states (see Sec. IID), (a) the variation of $\langle E_{A_1 A_2} \rangle$ with $E_{A_1 A_2 : B}$ remains non-monotonic and (b) with increasing N_1 , the states tend to the $\langle E_{A_1 A_2} \rangle = E_{A_1 A_2 : B}$ line. Also, increasing the non-Markovianity factor α generally tends to lower values of $\langle E_{A_1 A_2} \rangle$ and $E_{A_1 A_2 : B}$.

In the case of the gD states, our numerical investigation suggests that while the upper bound $\langle E_{A_1 A_2} \rangle \leq E_{A_1 A_2 : B}$ remains valid even in the presence of phase-flip noise irrespective of whether it is Markovian or non-Markovian. However, with increasing number of qubits, as in the case of the pure gD states, more states are concentrated close to the $\langle E_{A_1 A_2} \rangle = E_{A_1 A_2 : B}$ line, although the number of states for which $\langle E_{A_1 A_2} \rangle = E_{A_1 A_2 : B}$ diminishes drastically. This is demonstrated in Figs. 7(c) and 7(d) for gD states with $N = 3, 4$ qubits, respectively, under Markovian phase-flip noise. The results remain qualitatively the same even in the presence of non-Markovian phase-flip noise also.

c. Arbitrary pure states under noise. It is important to note that the numerical investigation for arbitrary N -qubit pure states subjected to phase-flip channels is resource intensive even for a small number of qubits due to the optimization involved in the computation of localizable entanglement, as the

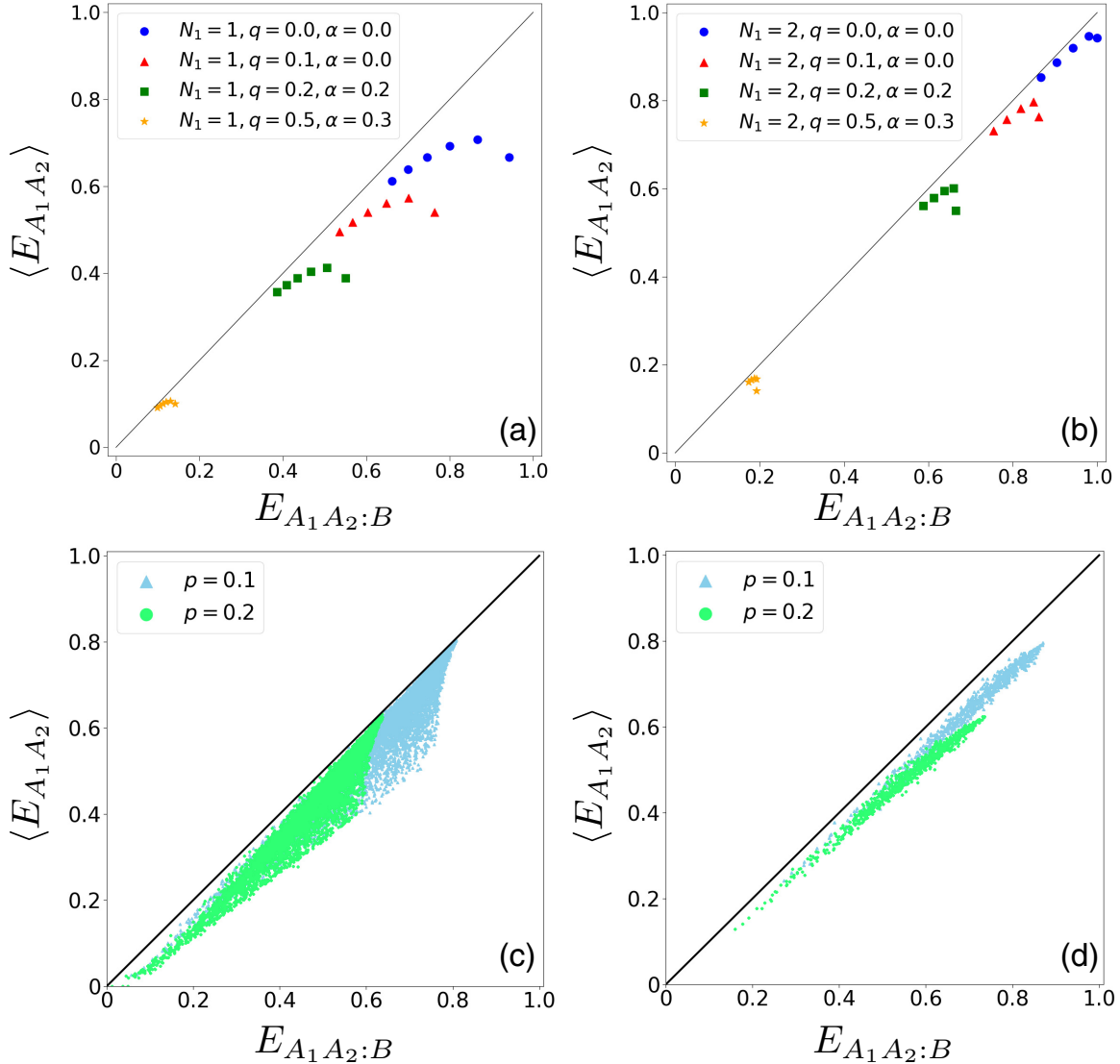


FIG. 7. Dicke and generalized Dicke states under phase-flip noise. (a), (b) Scatter plots of N -qubit Dicke states, for up to $N = 8$, under Markovian and non-Markovian phase-flip noise are shown on the $(E_{A_1 A_2 : B}, \langle E_{A_1 A_2} \rangle)$ planes for (a) $N_1 = 1$, and (b) $N_1 = 2$. (c), (d). On the other hand, scatter plots of samples of 10^7 gD states with (c) $N = 3$ and (d) $N = 4$ are shown on the $(E_{A_1 A_2 : B}, \langle E_{A_1 A_2} \rangle)$ plane. In all plots, negativity is used as entanglement measure. All quantities plotted in all figures are dimensionless.

number of optimization parameter increases with increasing n , the size of the measured subsystem B . In this paper, we restrict ourselves in reporting data for which B is constituted of one qubit only. Similar to the pure states of N qubits described in Sec. IID, we focus on δ_1 and δ_2 [Eqs. (63) and (64)] also for the mixed states obtained by subjecting N -qubit arbitrary pure states to Markovian phase-flip channels. As expected, for all investigated values of q , no states are found for which $\delta_2 \geq 0$, implying a violation of inequality (3), which is similar to the case of the pure states (see Sec. IID). On the other hand, the percentage of states for which $\delta_1 > 0$ are tabulated in Table I for different noise strengths in the case of the Markovian phase-flip channel. It is clear from the table that (a) for a fixed N with $n = 1$, the number of states for which $\delta_1 > 0$ overall decreases with increasing q , and (b) for a specific q value > 0 , such states overall decreases in number with increasing N , as long as n and m are fixed at 1.

It is important to note that the effect of single-qubit Pauli noise on localizable entanglement has been explored in literature [93,98], and a set of hierarchies between the localizable entanglement over a specific subsystem in a multiqubit state is proposed [98] in situations when local noise acts on either the subparts or on all the qubits of the whole system. In contrast, our work probes the multipartite systems subjected to single-qubit Pauli noise on all qubits via the bounds on localizable entanglement imposed by the entanglement present in the noisy system prior to measurement. We once again stress here that while we have used negativity as an entanglement measure to discuss the results in Sec. III, using other computable bipartite entanglement measures for mixed states, e.g., logarithmic negativity, yields qualitatively similar results, with changes only in the functional dependence of $\langle E_{A_1 A_2} \rangle$ on $E_{A_1 A_2 : B}$ and $\min\{E_{A_1 : A_2 B}, E_{A_2 : A_1 B}\}$, corresponding

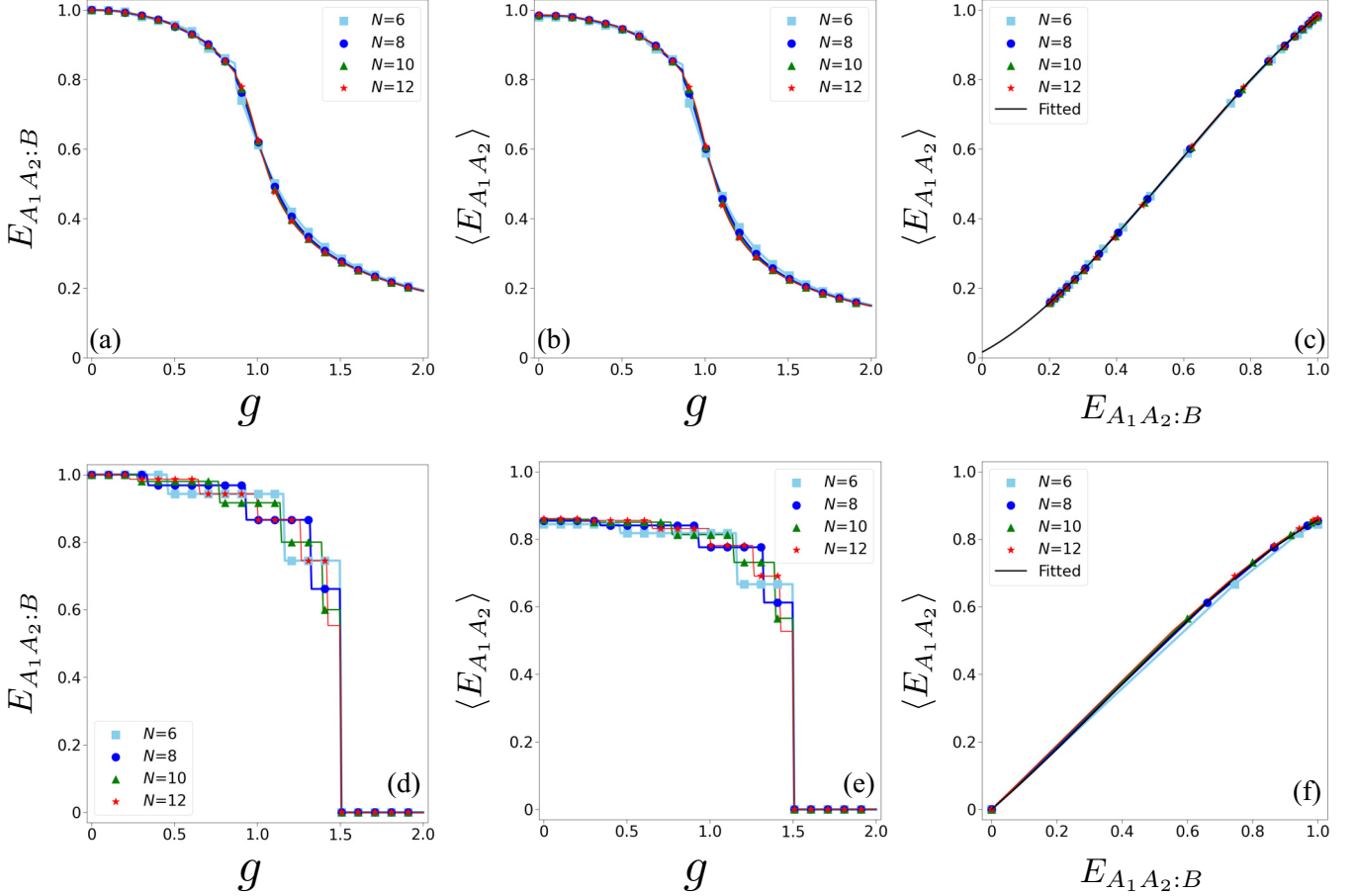


FIG. 8. Ordered 1D quantum spin models. Variations of $E_{A_1 A_2 : B}$ [(a), (d)] and $\langle E_{A_1 A_2} \rangle$ [(b), (e)] as functions of g for the TXY model [(a), (b)] and the XXZ model [(d), (e)] with different system sizes. (c), (f) Scatter plots of the ground states in 1D TXY model (c), and 1D XXZ model (f) in an external field on the $(E_{A_1 A_2 : B}, \langle E_{A_1 A_2} \rangle)$ plan. The variations of $\langle E_{A_1 A_2} \rangle$ as a function of $E_{A_1 A_2 : B}$ are fitted to Eq. (92) for both the 1D TXY model and the 1D XXZ model. In the case of the TXY model, γ is taken to be 0.5, while for the XXZ model, $\Delta = 0.5$. In this figure, we have used negativity to quantify entanglement. All quantities plotted in all figures are dimensionless.

to the bounds, and in the data presented in Table I, which exclusively correspond to negativity.

IV. INTERACTING 1D QUANTUM SPIN MODELS

It is natural to ask whether the bounds discussed in Sec. II for the pure states also exist in the ground states of paradigmatic quantum spin Hamiltonians. To investigate this, we focus on the 1D quantum spin chains with N spin-1/2 particles, governed by a Hamiltonian given by [79]

$$H = \sum_{i=1}^N \left[\frac{J_{i,i+1}^{xy}}{4} \{ (1 + \gamma) \sigma_i^x \sigma_{i+1}^x + (1 - \gamma) \sigma_i^y \sigma_{i+1}^y \} + \frac{J_{i,i+1}^{zz}}{4} \sigma_i^z \sigma_{i+1}^z + \frac{h_i}{2} \sigma_i^z \right]. \quad (91)$$

In Eq. (91), σ 's are Pauli operators, γ is the xy anisotropy parameter, h_i is local magnetic field strength corresponding to spin i , and $J_{i,i+1}^{xy}$ ($J_{i,i+1}^{zz}$) represents the nearest-neighbor xy (zz) interaction strengths. Also, we assume periodic boundary conditions (PBCs) in the system, implying $\sigma_{N+1}^{x,y,z} \equiv \sigma_1^{x,y,z}$. A number of paradigmatic 1D quantum spin models can be

represented by different special cases of H . In this paper, we are interested in two of them, namely, (a) TXY ($0 < \gamma \leq 1$, $J_{i,i+1}^{zz} = 0$) [69–74] (note that the transverse-field Ising model [73,74,99] is a special case of the TXY model with $\gamma = 1$), and (b) XXZ model with magnetic field (XXZ) ($\gamma = 0$) [75–80].

A. Ordered quantum spin models

In the case of the *ordered* quantum spin models where order exists in all spin-spin couplings as well as the field strengths, we assume $J_{i,i+1}^{xy} = J^{xy} > 0$, $J_{i,i+1}^{zz} = J^{zz} > 0$, and $h_i = h > 0$ for all $i = 1, 2, \dots, N$. In such models, we numerically investigate the correlation between $\langle E_{A_1 A_2} \rangle$ and $\{E_{A_1 A_2 : B}, E_{A_1 B : A_2}, E_{A_2 B : A_1}\}$ in the ground state, which is obtained via numerical diagonalization of H . We first consider the ordered antiferromagnetic (AFM) TXY model, and define $g = h/J^{xy}$ as the dimensionless field-strength. The model exhibits a quantum phase transition from an AFM phase ($g < 1$) to a paramagnetic (PM) phase ($g > 1$) at $g_c = 1$, for all values of $\gamma > 0$ [31,70–74,100,101]. Figures 8(a) and 8(b) depict the variations of $E_{A_1 A_2 : B}$ and $\langle E_{A_1 A_2} \rangle$, respectively, with negativity quantifying entanglement, as functions of g . The shape of the

TABLE II. Fitting parameters corresponding to Eq. (92) for the ordered TXY and XXZ model, with negativity, logarithmic negativity, and von Neumann entropy as entanglement measures. We have reported the error in the fitting iff the absolute value of the error $\geq 10^{-3}$.

TXY model.			
Parameters	Negativity	Logarithmic Negativity	von Neumann entropy
λ_0	0.015	0.058	-0.0064
λ_1	0.511	0.225	0.735
λ_2	1.087	1.516	0.703
λ_3	-0.629	-0.812	-0.454
XXZ model.			
Parameters	Negativity	Logarithmic Negativity	von Neumann entropy
λ_0	2.799×10^{-5}	0	0
λ_1	0.828	1.207 ± 0.001	0.786
λ_2	0.387 ± 0.002	-0.648 ± 0.008	0.611 ± 0.001
λ_3	-0.359	0.331 ± 0.002	-0.612

curve changes from convex to concave at $g = 1$, indicating that the absolute value of the first derivative of entanglement with respect to g exhibits a sharp peak at $g = 1$, signaling the quantum phase transition. Figure 8(c) presents the scatter plot of $\langle E_{A_1A_2} \rangle - E_{A_1A_2:B}$ corresponding to the ordered TXY model for different values of N using negativity, where for each N , values of $n, m = 1$. This, along with the PBC, ensures that $E_{A_1A_2:B} = E_{A_1:A_2B}$, while our numerical findings suggest that for the ground states of the TXY model with $n = m = 1$, $\min\{E_{A_1:A_2B}, E_{A_2:A_1B}\} = E_{A_1:A_2B}$ for all values of N . This implies that it is sufficient to investigate the dependence of $\langle E_{A_1A_2} \rangle$ on $E_{A_1A_2:B}$. It is evident from the figure that $\langle E_{A_1A_2} \rangle$ is positively correlated with $E_{A_1A_2:B}$. Irrespective of the value of N , the data suggests a cubic dependence of $\langle E_{A_1A_2} \rangle$ on $E_{A_1A_2:B}$, given by

$$\langle E_{A_1A_2} \rangle = \lambda_3 E_{A_1A_2:B}^3 + \lambda_2 E_{A_1A_2:B}^2 + \lambda_1 E_{A_1A_2:B} + \lambda_0, \quad (92)$$

where the values of $\lambda_{0,1,2,3}$ can be obtained by fitting the numerical data to Eq. (92) (see Table II). Note that at $g \rightarrow \infty$, both $E_{A_1A_2:B}$ and $\langle E_{A_1A_2} \rangle$ tend to vanish as the ground state of the TXY model becomes fully polarized. Therefore, one expects $\lambda_0 = 0$ in Eq. (92). However, we fit only the numerical data up to $g = 2$ to Eq. (92), which results in a small nonzero value of λ_0 . Our numerical investigation also suggests that the form of Eq. (92) remains invariant with a change in the values of the xy anisotropy parameter γ . Also, the qualitative results as well as the form (92) are invariant with a change in the entanglement measures, with a change only in the values of the fitting parameters. See Table II.

In the case of the XXZ model in a magnetic field along the z direction with PBCs, we assume $J^{zz} = \Delta J^{xy}$, where Δ signifies the z -anisotropy parameter, and denote the dimensionless field strength by $g = h/J^{xy}$. For $-1 \leq \Delta \leq 1$, the model undergoes a quantum phase transition from the XY phase to the ferromagnetic (FM) phase at the critical field strength $g_c = \pm(1 + \Delta)$ [79]. Similar to the TXY model, we

fix Δ and investigate the correlation between $\langle E_{A_1A_2} \rangle$ and $E_{A_1A_2:B}$. The data for the variations of $E_{A_1A_2:B}$ and $\langle E_{A_1A_2} \rangle$ with g using negativity are presented in Figs. 8(d) and 8(e), respectively, for $\Delta = 0.5$, where the quantum phase transition is indicated at $g_c = 1.5$ via a sharp fall in the value of entanglement. Figure 8(f) depicts the scatter plot of the points $(\langle E_{A_1A_2} \rangle, E_{A_1A_2:B})$ with negativity as entanglement measure, where the fitted curve has the same form as in Eq. (92). Note that in the case of the XXZ model in an external field, both $E_{A_1A_2:B}$ and $\langle E_{A_1A_2} \rangle$ reduces to zero for $g > 1.5$. Therefore, the $(E_{A_1A_2:B}, \langle E_{A_1A_2} \rangle)$ data includes the point (0,0), leading to $\lambda_0 = 0$ in the fitted curve. It is also worthwhile to note that in the case of the XXZ model, the overall relation between $\langle E_{A_1A_2} \rangle$ and $E_{A_1A_2:B}$ also remains unaltered with a change in the value of Δ within the mentioned region $-1 \leq \Delta \leq 1$. All these results for the XXZ model qualitatively remain the same if the choice of entanglement measure is changed, with only a change in the fitting parameters (see Table II). It is therefore clear from our numerical analysis that each of these 1D models can be classified by the variations of $\langle E_{A_1A_2} \rangle$ with $E_{A_1A_2:B}$, irrespective of the values of the system parameters as well as the system size.

B. Disordered quantum spin models

In a *disordered* quantum spin model [68], the values of a relevant system parameter, such as g , are chosen from a Gaussian distribution, $P(g)$, of fixed mean, $\langle g \rangle$, and fixed standard deviation, σ_g . Here, σ_g represents the *strength* of the disorder, and each random value of g represents a *random parameter configuration* of the quantum spin model, describing a *random realization* of the system. For each random realization of the system, the quantity of interest, $Q(g)$, can be computed. A subsequent *quenched* average of $Q(g)$ over a statistically large number of random realizations is given by

$$\langle Q \rangle_d = \int P(g)Q(g)dg, \quad (93)$$

where the subscript d represents a quenched average, and $\langle Q \rangle$ is effectively a function of $\langle g \rangle$ and σ_g . Note that the corresponding *ordered* result can be obtained as a special case at $\sigma_g = 0$. Note also that disorder can, in principle, be present in a number of system parameters. In this paper, however, we confine ourselves in situations where only one chosen system parameter is disordered.

We start with the TXY model, choosing the field strength h (and hence g , where J^{xy} is constant) to be the disordered system parameter. The quenched averaged localizable entanglement, $\langle \langle E_{A_1A_2} \rangle \rangle_d$, and the bipartite entanglement, $\langle E_{A_1A_2:B} \rangle_d$, quantified using negativity, in the ground state of the system are numerically computed for different values of the disorder strength σ_g , and are plotted against $\langle g \rangle$ in Figs. 9(a) and 9(b). In each of these computations on an N -qubit system, both n and m are taken to be 1, similar to the ordered scenario. Figure 9(c), on the other hand, represents the scatter plots of the ground state of the 1D disordered TXY model on the $(\langle \langle E_{A_1A_2} \rangle \rangle_d - \langle E_{A_1A_2:B} \rangle_d)$ plane using negativity, where the numerical data is found to be well-fitted to Eq. (92) with $\lambda_0 = 0.014$, $\lambda_1 = 0.520$, $\lambda_2 = 1.065$, and $\lambda_3 = -0.617$, where errors $\leq 10^{-3}$ are neglected. This indicates that the

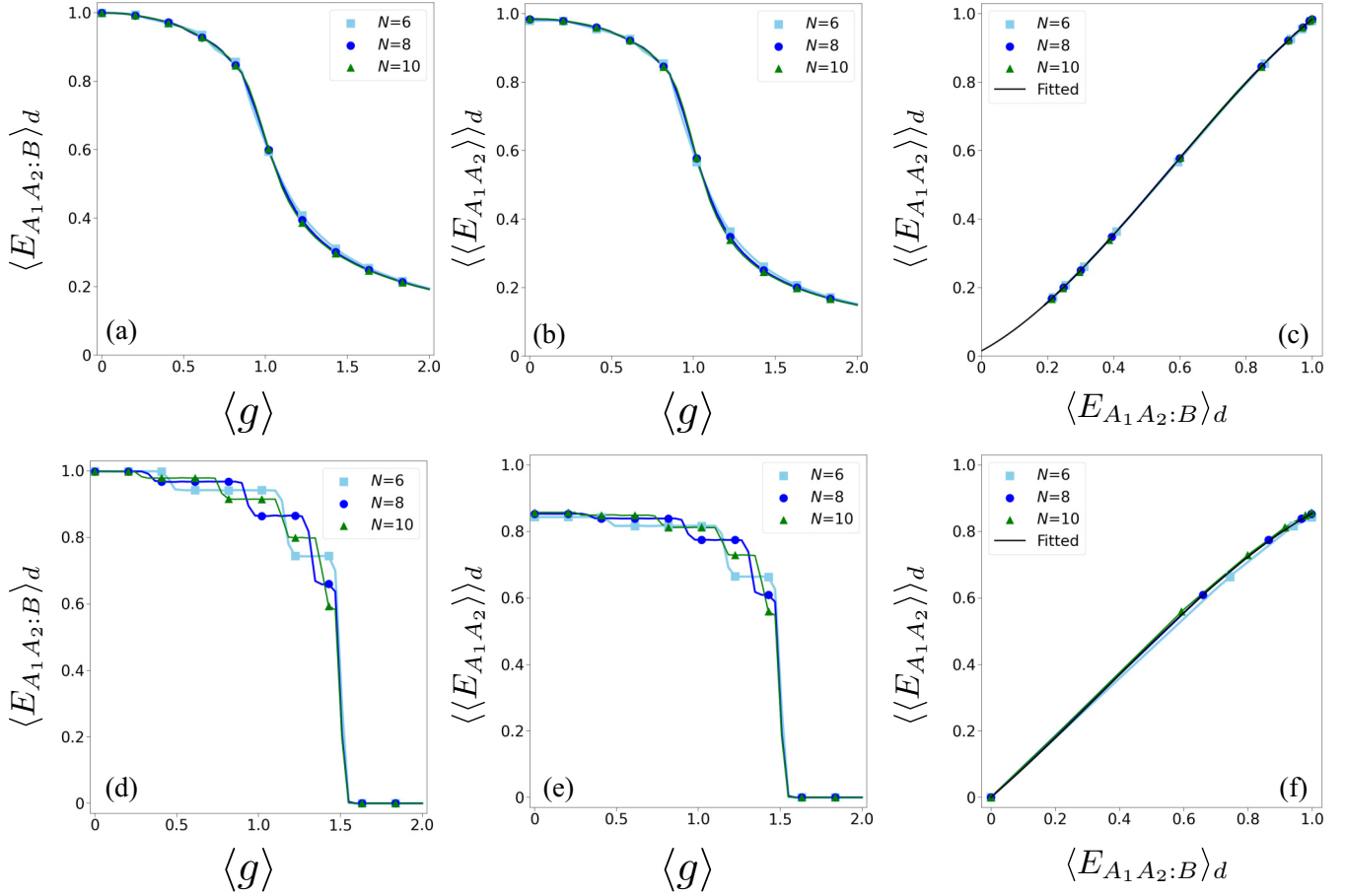


FIG. 9. Disordered 1D quantum spin models. Variations of $\langle E_{A_1 A_2 : B} \rangle_d$ [(a), (d)] and $\langle \langle E_{A_1 A_2} \rangle \rangle_d$ [(b), (e)] as functions of $\langle g \rangle$ for the TXY model [(a), (b)] and the XXZ model [(d), (e)] with different system sizes. (c), (f) Scatter plots of the ground states in 1D TXY model (c), and 1D XXZ model (f) in an external field on the $(\langle E_{A_1 A_2 : B} \rangle_d, \langle \langle E_{A_1 A_2} \rangle \rangle_d)$ plane. The variations of $\langle \langle E_{A_1 A_2} \rangle \rangle_d$ as a function of $\langle E_{A_1 A_2 : B} \rangle_d$ are fitted to Eq. (92) for both the 1D TXY model and the 1D XXZ model. In the case of the TXY model, γ is taken to be 0.5, while for the XXZ model, $\Delta = 0.5$. For all cases, $\sigma_g = 0.05$. In this figure, we have used negativity to quantify entanglement. All quantities plotted in all figures are dimensionless.

relation between $\langle E_{A_1 A_2} \rangle$ and $E_{A_1 A_2 : B}$ for the TXY model is qualitatively robust against disorder in the field. Also, varying σ_g in the range $0.01 \leq \sigma_g \leq 0.1$ only changes the fitting parameters negligibly. Similar analysis is performed for the XXZ model in an external field to arrive at a similar conclusion, where the data corresponding to negativity is presented in Figs. 9(d)–9(f). Also, similar to the ordered case, all of these results remain qualitatively unchanged with a change in the entanglement measure.

V. CONCLUSIONS AND OUTLOOK

In this paper, we investigate dependence of the gain in the entanglement through localization over a group of qubits in a multiqubit system via single-qubit projection measurements on the rest of the qubits on the amount of loss in bipartite entanglement during these measurements. We probe a number of paradigmatic N -qubit pure states, namely, the generalized GHZ, generalized W , Dicke, and the gD states. We derive analytical bounds for the generalized GHZ and the generalized W states. We show that the gain is always equal to the loss in the former, while in the latter, lower and upper bounds

of localizable entanglement can be derived in terms of the bipartite entanglement present in the system prior to the measurement process. In the case of the Dicke and the gD states, a combination of analytical and numerical investigations reveal that the localizable entanglement tend to be equal to a component of the lost bipartite entanglement when the number of qubits increases. Modifications of these results, when the system is subjected to single-qubit Markovian and non-Markovian phase-flip channels, are also discussed. We extend our study to the ground states of the 1D quantum spin models, namely, the TXY model and the XXZ model in an external field, and numerically demonstrate a cubic dependence of the localizable entanglement over the bipartite entanglement in the ground state prior to measurement, where measurement is restricted to one qubit only, and the entanglement is always computed in the 1:rest bipartition. This dependence is shown to be qualitatively robust even in the presence of disorder in the field strength.

A number of possible avenues of future research emerge from this paper. Within the orbit of results reported in this paper, it is important to understand how the results obtained in the case of the pure states are modified when different types

of noise that commonly occur in experiments [102,103], such as the bit-flip, depolarizing, and amplitude-damping [62,63] noise, are present in the system. However, investigating such noise channels may present new challenges in deriving the appropriate bounds, if any, on localizable entanglement. Also, in the case of the 1D quantum spin systems considered in this paper, it would be interesting to see the effect of the presence of disorder in the spin-spin interaction strengths along with a disordered field-strength. In addition, a plethora of quantum spin models are important from the perspective of quantum information theory [31,32], and it would be interesting to investigate whether a specific relation between the localized and the lost entanglement, similar to the one in the case of the models described in this paper, exist in the ground states of these models in the presence and absence of disordered interactions, as well as in situations where the system is made open by allowing an interaction with the environment [104].

ACKNOWLEDGMENTS

We acknowledge the use of QIClib [105]—a modern C++ library for general purpose quantum information processing and quantum computing.

APPENDIX A: ENTANGLEMENT MEASURES

Here we define the entanglement measures used in this paper. The amount of entanglement between two partitions A and B of a bipartite quantum state ρ_{AB} can be quantified by a bipartite entanglement measure [1,2]. In this paper, for both pure as well as mixed states, we focus on negativity [81–85] as a bipartite entanglement measure, which is defined as

$$E_{A:B}^{neg} = \|\rho_{AB}^{T_B}\| - 1, \quad (\text{A1})$$

which corresponds to the absolute value of the sum of negative eigenvalues, λ , of $\rho_{AB}^{T_B}$, given by

$$E_{A:B}^{neg} = 2 \left| \sum_{\lambda_i < 0} \lambda_i \right|. \quad (\text{A2})$$

Here, $\|\varrho\| = \text{Tr}\sqrt{\varrho^\dagger\varrho}$ is the trace norm of the density operator ϱ , computed as the sum of the singular values of ϱ . The matrix $\rho_{AB}^{T_B}$ is obtained by performing partial transposition of the density matrix ρ_{AB} with respect to subsystem B . Since we only focus on negativity throughout this paper, we discard the superscript from $E_{A:B}^{neg}$, and denote the negativity between partitions A and B by $E_{A:B}$. One can also define the *logarithmic negativity* [89] $\mathcal{L}_{A:B}$ over the same partitions $A : B$ as

$$\mathcal{L}_{A:B} = \log_2(E_{A:B} + 1). \quad (\text{A3})$$

In the case of a pure bipartite state ρ_{AB} , the entanglement over bipartition $A : B$ can also be quantified by the von Neumann entropy [1,2,82,90,91] of the reduced density matrix $\rho_A = \text{Tr}_B(\rho_{AB})$ as

$$S = -\rho_A \log_2 \rho_A = -\sum_{\lambda} \lambda \log_2 \lambda, \quad (\text{A4})$$

where $\{\lambda\}$ are the eigenvalues of ρ_A .

APPENDIX B: SINGLE- AND TWO-QUBIT MEASUREMENTS

We first consider the single-qubit measurement ($n = 1$) in an N -qubit gW state, where [see Eq. (22)]

$$f_0^0 = a_1 e^{-i\phi} \sin \frac{\theta}{2}, \quad f_1^0 = -a_1 e^{-i\phi} \cos \frac{\theta}{2}, \quad (\text{B1})$$

$$f^0 = \cos \frac{\theta}{2}, \quad f^1 = \sin \frac{\theta}{2}, \quad (\text{B2})$$

and

$$p_0 = a_1^2 \sin^2 \frac{\theta}{2} + \cos^2 \frac{\theta}{2} \sum_{i=1}^{N-1} a_{1+i}^2,$$

$$p_1 = a_1^2 \cos^2 \frac{\theta}{2} + \sin^2 \frac{\theta}{2} \sum_{i=1}^{N-1} a_{1+i}^2, \quad (\text{B3})$$

such that $\langle \psi_k | \psi_k \rangle = 1$ for $k = 0, 1$. On the other hand, in the case of two-qubit projection measurements ($n = 2$) on an N -qubit gW state, the postmeasured states are of the form given in Eq. (22), with the coefficients f_0^k 's and f^k 's as

$$\begin{aligned} f_0^0 &= a_1 e^{-i\phi_1} \sin \frac{\theta_1}{2} \cos \frac{\theta_2}{2} + a_2 e^{-i\phi_2} \cos \frac{\theta_1}{2} \sin \frac{\theta_2}{2}, & f_1^0 &= a_1 e^{-i\phi_1} \sin \frac{\theta_1}{2} \sin \frac{\theta_2}{2} - a_2 e^{-i\phi_2} \cos \frac{\theta_1}{2} \cos \frac{\theta_2}{2}, \\ f_0^2 &= -a_1 e^{-i\phi_1} \cos \frac{\theta_1}{2} \cos \frac{\theta_2}{2} + a_2 e^{-i\phi_2} \sin \frac{\theta_1}{2} \sin \frac{\theta_2}{2}, & f_1^2 &= -a_1 e^{-i\phi_1} \cos \frac{\theta_1}{2} \sin \frac{\theta_2}{2} - a_2 e^{-i\phi_2} \sin \frac{\theta_1}{2} \cos \frac{\theta_2}{2}, \end{aligned} \quad (\text{B4})$$

and

$$f^0 = \cos \frac{\theta_1}{2} \cos \frac{\theta_2}{2}, \quad f^1 = \cos \frac{\theta_1}{2} \sin \frac{\theta_2}{2}, \quad f^2 = \sin \frac{\theta_1}{2} \cos \frac{\theta_2}{2}, \quad f^3 = \sin \frac{\theta_1}{2} \sin \frac{\theta_2}{2}. \quad (\text{B5})$$

The probabilities of obtaining the measurement outcome $k = 0, 1, 2, 3$ are given by

$$\begin{aligned} p_0 &= a_1^2 \sin^2 \frac{\theta_1}{2} \cos^2 \frac{\theta_2}{2} + a_2^2 \cos^2 \frac{\theta_1}{2} \sin^2 \frac{\theta_2}{2} + \cos^2 \frac{\theta_1}{2} \cos^2 \frac{\theta_2}{2} \sum_{i=1}^{N-2} a_{2+i}^2, \\ p_1 &= a_1^2 \sin^2 \frac{\theta_1}{2} \sin^2 \frac{\theta_2}{2} + a_2^2 \cos^2 \frac{\theta_1}{2} \cos^2 \frac{\theta_2}{2} + \cos^2 \frac{\theta_1}{2} \sin^2 \frac{\theta_2}{2} \sum_{i=1}^{N-2} a_{2+i}^2, \end{aligned}$$

$$\begin{aligned}
p_2 &= a_1^2 \cos^2 \frac{\theta_1}{2} \cos^2 \frac{\theta_2}{2} + a_2^2 \sin^2 \frac{\theta_1}{2} \sin^2 \frac{\theta_2}{2} + \sin^2 \frac{\theta_1}{2} \cos^2 \frac{\theta_2}{2} \sum_{i=1}^{N-2} a_{2+i}^2, \\
p_3 &= a_1^2 \cos^2 \frac{\theta_1}{2} \sin^2 \frac{\theta_2}{2} + a_2^2 \sin^2 \frac{\theta_1}{2} \cos^2 \frac{\theta_2}{2} + \sin^2 \frac{\theta_1}{2} \sin^2 \frac{\theta_2}{2} \sum_{i=1}^{N-2} a_{2+i}^2.
\end{aligned} \tag{B6}$$

For a three-qubit state belonging to the W class [see Eq. (50)], measurement on qubit 1 can be described in a way similar to that for the three-qubit gW state, with f_0^k ($k = 0, 1$) given by

$$\begin{aligned}
f_0^0 &= a_0 \cos \frac{\theta}{2} + a_1 e^{-i\phi} \sin \frac{\theta}{2}, \\
f_0^1 &= a_0 \sin \frac{\theta}{2} - a_1 e^{-i\phi} \cos \frac{\theta}{2},
\end{aligned} \tag{B7}$$

and f^k ($k = 0, 1$), given by

$$f^0 = \cos \frac{\theta}{2}, \quad f^1 = \sin \frac{\theta}{2} \tag{B8}$$

and

$$\begin{aligned}
p_0 &= \left| a_0 \cos \frac{\theta}{2} + a_1 e^{-i\phi} \sin \frac{\theta}{2} \right|^2 + (a_2^2 + a_3^2) \cos^2 \frac{\theta}{2}, \\
p_1 &= \left| a_0 \sin \frac{\theta}{2} - a_1 e^{-i\phi} \cos \frac{\theta}{2} \right|^2 + (a_2^2 + a_3^2) \sin^2 \frac{\theta}{2}.
\end{aligned} \tag{B9}$$

APPENDIX C: THREE-QUBIT GW STATES WITH COMPLEX COEFFICIENTS

Here, we present the crucial steps for computing the localizable entanglement over qubits 2 and 3 in a three-qubit gW state $|\psi\rangle = a_1|100\rangle + a_2|010\rangle + a_3|001\rangle$ [Eq. (19) with $N = 3$] with complex coefficients a_1, a_2 , and a_3 , via a measurement on qubit 1. The postmeasured states $|\psi_k\rangle$ [Eq. (22)] are given by $|\psi_k\rangle = c_0^k|00\rangle + c_1^k|01\rangle + c_2^k|10\rangle$, $k = 1, 2$, such that $|c_0^k|^2 + |c_1^k|^2 + |c_2^k|^2 = 1$, where the forms of c_i^k , $i = 0, 1, 2$, $k = 1, 2$ are given in Sec. II B. The state $|\psi_k\rangle\langle\psi_k|$, upon partial transposition, becomes

$$\begin{bmatrix} |c_0^k|^2 & c_1^k c_0^{k*} & c_0^k c_2^{k*} & c_1^k c_2^{k*} \\ c_0^k c_1^{k*} & |c_1^k|^2 & 0 & 0 \\ c_2^k a c_0^{k*} & 0 & |c_2^k|^2 & 0 \\ c_2^k c_1^{k*} & 0 & 0 & 0 \end{bmatrix}, \tag{C1}$$

having the eigenvalues

$$\begin{aligned}
\lambda_0 &= -|c_1^k||c_2^k|, \\
\lambda_1 &= |c_1^k||c_2^k|, \\
\lambda_2 &= \frac{1}{2}(1 - \sqrt{1 - 4|c_1^k|^2|c_2^k|^2}), \\
\lambda_3 &= \frac{1}{2}(1 + \sqrt{1 - 4|c_1^k|^2|c_2^k|^2}),
\end{aligned} \tag{C2}$$

among which only λ_0 is negative. Therefore, $\langle E_{23}^k \rangle = |c_1^k||c_2^k|$. On the other hand, partial transpose of the state $|\psi\rangle\langle\psi|$ with respect to the bipartition 1 : 23 followed by a diagonalization

leads to the nonzero eigenvalues

$$\begin{aligned}
\lambda_0 &= |a_1|^2, \\
\lambda_1 &= -|a_1|\sqrt{|a_2|^2 + |a_3|^2}, \\
\lambda_2 &= |a_1|\sqrt{|a_2|^2 + |a_3|^2}, \\
\lambda_3 &= |a_2|^2 + |a_3|^2,
\end{aligned} \tag{C3}$$

leading to $E_{1:23} = |a_1|\sqrt{|a_2|^2 + |a_3|^2}$. Replacing c_i^k as per definition in terms of a_i in $\langle E_{23} \rangle$ and using $E_{1:23}$, one can arrive at Propositions II and III and the corresponding corollaries.

APPENDIX D: SPECIFIC EXAMPLES

In this Appendix, we demonstrate a number of results discussed in Secs. II and III using specific examples.

a. Upper bound for gW states. Consider the cases of $N = 3, 4$, for which the family of states providing the upper bound of $\langle E_{A_1 A_2} \rangle$ in the case of gW states with real coefficients can be written as

$$|\Psi_3\rangle = a|100\rangle + \sqrt{\frac{1-a^2}{2}}(|010\rangle + |001\rangle), \tag{D1}$$

$$\begin{aligned}
|\Psi_4\rangle &= a|1000\rangle + \sqrt{\frac{1-a^2}{2}}|0100\rangle + b|0010\rangle \\
&\quad + \sqrt{\frac{1-a^2-2b^2}{2}}|0001\rangle,
\end{aligned} \tag{D2}$$

where a, b are real numbers. The behavior of $\langle E_{A_1 A_2} \rangle$ as a function of a, b is shown in Figs. 2(a) and 2(b). Also, $\langle E_{A_1 A_2} \rangle$ for the state $|\Psi_3\rangle$ provides an upper bound for $\langle E_{A_1 A_2} \rangle$ corresponding to all three-qubit gW states with complex coefficients. This is demonstrated by the $\langle E_{A_1 A_2} \rangle$ values corresponding to 10^6 Haar uniformly generated three-qubit gW states lying below the upper bound.

b. Maximum bipartite entanglement for gW states. The line $E_{A_1 A_2 : B} = 1$ corresponds to the family of states given by

$$\sum_{i \in B} a_i^2 = \left(4 \sum_{i \in A} a_i^2 \right)^{-1}. \tag{D3}$$

Specifically, for a three-qubit system, this family is given by

$$|\Phi_3\rangle = \sqrt{\frac{1}{2}}|100\rangle + a|010\rangle + \sqrt{\frac{1}{2} - a^2}|001\rangle, \tag{D4}$$

while for $N = 4, n = m = 1$,

$$\begin{aligned}
|\Phi_4\rangle &= \sqrt{\frac{1}{2}}|1000\rangle + a|0100\rangle + b|0010\rangle \\
&\quad + \sqrt{\frac{1}{2} - a^2 - b^2}|0001\rangle.
\end{aligned} \tag{D5}$$

- [1] R. Horodecki, P. Horodecki, M. Horodecki, and K. Horodecki, Quantum entanglement, *Rev. Mod. Phys.* **81**, 865 (2009).
- [2] O. Gühne and G. Tóth, Entanglement detection, *Phys. Rep.* **474**, 1 (2009).
- [3] C. H. Bennett, G. Brassard, C. Crépeau, R. Jozsa, A. Peres, and W. K. Wootters, Teleporting an Unknown Quantum State Via Dual Classical and Einstein-Podolsky-Rosen Channels, *Phys. Rev. Lett.* **70**, 1895 (1993).
- [4] D. Bouwmeester, J.-W. Pan, K. Mattle, M. Eibl, H. Weinfurter, and A. Zeilinger, Experimental quantum teleportation, *Nature* **390**, 575 (1997).
- [5] C. H. Bennett and S. J. Wiesner, Communication Via One- and Two-Particle Operators on Einstein-Podolsky-Rosen States, *Phys. Rev. Lett.* **69**, 2881 (1992).
- [6] K. Mattle, H. Weinfurter, P. G. Kwiat, and A. Zeilinger, Dense Coding in Experimental Quantum Communication, *Phys. Rev. Lett.* **76**, 4656 (1996).
- [7] A. Sen(De) and U. Sen, Quantum advantage in communication networks, [arXiv:1105.2412v1](https://arxiv.org/abs/1105.2412v1).
- [8] A. K. Ekert, Quantum Cryptography Based on Bell's Theorem, *Phys. Rev. Lett.* **67**, 661 (1991).
- [9] T. Jennewein, C. Simon, G. Weihs, H. Weinfurter, and A. Zeilinger, Quantum Cryptography with Entangled Photons, *Phys. Rev. Lett.* **84**, 4729 (2000).
- [10] V. E. Hubeny, The AdS/CFT correspondence, *Class. Quantum Grav.* **32**, 124010 (2015).
- [11] F. Pastawski, B. Yoshida, D. Harlow, and J. Preskill, Holographic quantum error-correcting codes: Toy models for the bulk/boundary correspondence, *J. High Energy Phys.* **06** (2015) 149.
- [12] A. Almheiri, X. Dong, and D. Harlow, Bulk locality and quantum error correction in AdS/CFT, *J. High Energy Phys.* **04** (2015) 163.
- [13] A. Jahn, M. Gluza, F. Pastawski, and J. Eisert, Holography and criticality in matchgate tensor networks, *Sci. Adv.* **5**, eaaw0092 (2019).
- [14] D. N. Page and W. K. Wootters, Evolution without evolution: Dynamics described by stationary observables, *Phys. Rev. D* **27**, 2885 (1983).
- [15] R. Gambini, R. A. Porto, J. Pullin, and S. Torterolo, Conditional probabilities with dirac observables and the problem of time in quantum gravity, *Phys. Rev. D* **79**, 041501(R) (2009).
- [16] E. Moreva, G. Brida, M. Gramegna, V. Giovannetti, L. Maccone, and M. Genovese, Time from quantum entanglement: An experimental illustration, *Phys. Rev. A* **89**, 052122 (2014).
- [17] N. Lambert, Y.-N. Chen, Y. C. Cheng, C.-M. Li, G. Y. Chen, and F. Nori, Quantum biology, *Nat. Phys.* **9**, 10 (2013).
- [18] J. M. Raimond, M. Brune, and S. Haroche, Manipulating quantum entanglement with atoms and photons in a cavity, *Rev. Mod. Phys.* **73**, 565 (2001).
- [19] R. Prevedel, G. Cronenberg, M. S. Tame, M. Paternostro, P. Walther, M. S. Kim, and A. Zeilinger, Experimental Realization of Dicke States of Up to Six Qubits for Multiparty Quantum Networking, *Phys. Rev. Lett.* **103**, 020503 (2009).
- [20] S. Barz, Quantum computing with photons: Introduction to the circuit model, the one-way quantum computer, and the fundamental principles of photonic experiments, *J. Phys. B: At. Mol. Opt. Phys.* **48**, 083001 (2015).
- [21] D. Leibfried, R. Blatt, C. Monroe, and D. Wineland, Quantum dynamics of single trapped ions, *Rev. Mod. Phys.* **75**, 281 (2003).
- [22] D. Leibfried, E. Knill, S. Seidelin, J. Britton, R. B. Blakestad, J. Chiaverini, D. B. Hume, W. M. Itano, J. D. Jost, C. Langer, R. Ozeri, R. Reichle, and D. J. Wineland, Creation of a six-atom 'Schrödinger cat' state, *Nature* **438**, 639 (2005).
- [23] K. R. Brown, J. Kim, and C. Monroe, Co-designing a scalable quantum computer with trapped atomic ions, *Nat. Phys. J. Quant. Inf.* **2**, 16034 (2016).
- [24] O. Mandel, M. Greiner, A. Widera, T. Rom, T. W. Hansch, and I. Bloch, Controlled collisions for multi-particle entanglement of optically trapped atoms, *Nature* **425**, 937 (2003).
- [25] I. Bloch, Exploring quantum matter with ultracold atoms in optical lattices, *J. Phys. B: At. Mol. Opt. Phys.* **38**, S629 (2005).
- [26] I. Bloch, J. Dalibard, and W. Zwerger, Many-body physics with ultracold gases, *Rev. Mod. Phys.* **80**, 885 (2008).
- [27] J. Clarke and F. K. Wilhelm, Superconducting quantum bits, *Nature* **453**, 1031 (2008).
- [28] R. Barends, J. Kelly, A. Megrant, A. Veitia, D. Sank, E. Jeffrey, T. C. White, J. Mutus, A. G. Fowler, B. Campbell, Y. Chen, Z. Chen, B. Chiaro, A. Dunsworth, C. Neill, P. O'Malley, P. Roushan, A. Vainsencher, J. Wenner, A. N. Korotkov *et al.*, Superconducting quantum circuits at the surface code threshold for fault tolerance, *Nature* **508**, 500 (2014).
- [29] C. Negrevergne, T. S. Mahesh, C. A. Ryan, M. Ditty, F. Cyrcacine, W. Power, N. Boulant, T. Havel, D. G. Cory, and R. Laflamme, Benchmarking Quantum Control Methods on a 12-Qubit System, *Phys. Rev. Lett.* **96**, 170501 (2006).
- [30] R. Augusiak, F. M. Cucchietti, and M. Lewenstein, Many-body physics from a quantum information perspective, in *Modern Theories of Many-Particle Systems in Condensed Matter Physics*, edited by D. C. Cabra, A. Honecker, and P. Pujol (Springer, Berlin, 2012), pp. 245–294.
- [31] L. Amico, R. Fazio, A. Osterloh, and V. Vedral, Entanglement in many-body systems, *Rev. Mod. Phys.* **80**, 517 (2008).
- [32] G. De Chiara and A. Sanpera, *Rep. Prog. Phys.* **81**, 074002 (2018).
- [33] M. Horodecki, Entanglement measures, *Quantum Inf. Comput.* **1**, 3 (2001).
- [34] D. M. Greenberger, M. A. Horne, and A. Zeilinger, *Bell's Theorem, Quantum Theory and Conceptions of the Universe* (Kluwer, Netherlands, 1989).
- [35] M. Hein, W. Dür, J. Eisert, R. Raussendorf, M. Van den Nest, and H.-J. Briegel, Entanglement in graph states and its applications, [arXiv:quant-ph/0602096](https://arxiv.org/abs/quant-ph/0602096).
- [36] R. Raussendorf, D. E. Browne, and H. J. Briegel, Measurement-based quantum computation on cluster states, *Phys. Rev. A* **68**, 022312 (2003).
- [37] K. Fujii, Quantum computation with topological codes: from qubit to topological fault-tolerance, [arXiv:1504.01444](https://arxiv.org/abs/1504.01444).
- [38] D. P. DiVincenzo, C. A. Fuchs, H. Mabuchi, J. A. Smolin, A. Thapliyal, and A. Uhlmann, Entanglement of assistance, [arXiv:quant-ph/9803033](https://arxiv.org/abs/quant-ph/9803033).
- [39] F. Verstraete, M. Popp, and J. I. Cirac, Entanglement Versus Correlations in Spin Systems, *Phys. Rev. Lett.* **92**, 027901 (2004).

- [40] F. Verstraete, M. A. Martín-Delgado, and J. I. Cirac, Diverging Entanglement Length in Gapped Quantum Spin Systems, *Phys. Rev. Lett.* **92**, 087201 (2004).
- [41] M. Popp, F. Verstraete, M. A. Martín-Delgado, and J. I. Cirac, Localizable entanglement, *Phys. Rev. A* **71**, 042306 (2005).
- [42] D. Sadhukhan, S. S. Roy, A. K. Pal, D. Rakshit, A. Sen(De), and U. Sen, Multipartite entanglement accumulation in quantum states: Localizable generalized geometric measure, *Phys. Rev. A* **95**, 022301 (2017).
- [43] D. Amaro, M. Müller, and A. K. Pal, Estimating localizable entanglement from witnesses, *New J. Phys.* **20**, 063017 (2018).
- [44] D. Amaro, M. Müller, and A. K. Pal, Scalable characterization of localizable entanglement in noisy topological quantum codes, *New J. Phys.* **22**, 053038 (2020).
- [45] B.-Q. Jin and V. E. Korepin, Localizable entanglement in antiferromagnetic spin chains, *Phys. Rev. A* **69**, 062314 (2004).
- [46] S. O. Skrøvseth and S. D. Bartlett, Phase transitions and localizable entanglement in cluster-state spin chains with Ising couplings and local fields, *Phys. Rev. A* **80**, 022316 (2009).
- [47] P. Smacchia, L. Amico, P. Facchi, R. Fazio, G. Florio, S. Pascazio, and V. Vedral, Statistical mechanics of the cluster Ising model, *Phys. Rev. A* **84**, 022304 (2011).
- [48] S. Montes and A. Hamma, Phase diagram and quench dynamics of the cluster-xy spin chain, *Phys. Rev. E* **86**, 021101 (2012).
- [49] A. Acín, J. I. Cirac, and M. Lewenstein, Entanglement percolation in quantum networks, *Nat. Phys.* **3**, 256 (2007).
- [50] S. Popescu and D. Rohrlich, Thermodynamics and the measure of entanglement, *Phys. Rev. A* **56**, R3319 (1997).
- [51] V. Vedral and M. B. Plenio, Entanglement measures and purification procedures, *Phys. Rev. A* **57**, 1619 (1998).
- [52] G. Vidal, Entanglement monotones, *J. Mod. Opt.* **47**, 355 (2000).
- [53] J. A. Smolin, F. Verstraete, and A. Winter, Entanglement of assistance and multipartite state distillation, *Phys. Rev. A* **72**, 052317 (2005).
- [54] D. Yang and J. Eisert, Entanglement Combing, *Phys. Rev. Lett.* **103**, 220501 (2009).
- [55] K. Pollock, G. Wang, and E. Chitambar, Entanglement of assistance in three-qubit systems, *Phys. Rev. A* **103**, 032428 (2021).
- [56] W. Dür, G. Vidal, and J. I. Cirac, Three qubits can be entangled in two inequivalent ways, *Phys. Rev. A* **62**, 062314 (2000).
- [57] A. Sen(De), U. Sen, M. Wieśniak, D. Kaszlikowski, and M. Żukowski, Multiqubit W states lead to stronger nonclassicality than Greenberger-Horne-Zeilinger states, *Phys. Rev. A* **68**, 062306 (2003).
- [58] R. H. Dicke, Coherence in spontaneous radiation processes, *Phys. Rev.* **93**, 99 (1954).
- [59] M. Bergmann and O. Gühne, Entanglement criteria for Dicke states, *J. Phys. A: Math. Theor.* **46**, 385304 (2013).
- [60] B. Lücke, J. Peise, G. Vitagliano, J. Arlt, L. Santos, G. Tóth, and C. Klempt, Detecting Multipartite Entanglement of Dicke States, *Phys. Rev. Lett.* **112**, 155304 (2014).
- [61] A. Kumar, H. S. Dhar, R. Prabhu, A. Sen(De), and U. Sen, Forbidden regimes in the distribution of bipartite quantum correlations due to multiparty entanglement, *Phys. Lett. A* **381**, 1701 (2017).
- [62] M. A. Nielsen and I. L. Chuang, *Quantum Computation and Quantum Information* (Cambridge University Press, Cambridge, UK, 2010).
- [63] A. S. Holevo and V. Giovannetti, Quantum channels and their entropic characteristics, *Rep. Prog. Phys.* **75**, 046001 (2012).
- [64] T. Yu and J. H. Eberly, Sudden death of entanglement, *Science* **323**, 598 (2009).
- [65] S. Daffer, K. Wódkiewicz, J. D. Cresser, and J. K. McIver, Depolarizing channel as a completely positive map with memory, *Phys. Rev. A* **70**, 010304(R) (2004).
- [66] U. Shrikant, R. Srikanth, and S. Banerjee, Non-Markovian dephasing and depolarizing channels, *Phys. Rev. A* **98**, 032328 (2018).
- [67] R. Gupta, S. Gupta, S. Mal, A. Sen(De), and U. Sen, Constructive feedback of non-Markovianity on resources in random quantum states, *Phys. Rev. A* **105**, 012424 (2022).
- [68] C. De Dominicis and I. Giardinà, *Random Fields and Spin Glasses: A Field Theory Approach* (Cambridge University Press, Cambridge, UK, 2006).
- [69] E. Lieb, T. Schultz, and D. Mattis, Two soluble models of an antiferromagnetic chain, *Ann. Phys.* **16**, 407 (1961).
- [70] E. Barouch, B. M. McCoy, and M. Dresden, Statistical mechanics of the XY model. I, *Phys. Rev. A* **2**, 1075 (1970).
- [71] E. Barouch and B. M. McCoy, Statistical mechanics of the XY model. II. Spin-correlation functions, *Phys. Rev. A* **3**, 786 (1971).
- [72] E. Barouch and B. M. McCoy, Statistical mechanics of the XY model. III, *Phys. Rev. A* **3**, 2137 (1971).
- [73] B. K. Chakrabarti, A. Dutta, and P. Sen, *Quantum Ising Phases and Transitions in Transverse Ising Models* (Springer, Heidelberg, Berlin Heidelberg, 1996), Vol. 41.
- [74] Subir Sachdev, *Quantum Phase Transitions*, 2nd ed. (Cambridge University Press, Cambridge, UK, 2011).
- [75] C. N. Yang and C. P. Yang, One-dimensional chain of anisotropic spin-spin interactions. I. Proof of Bethe's hypothesis for ground state in a finite system, *Phys. Rev.* **150**, 321 (1966).
- [76] C. N. Yang and C. P. Yang, One-dimensional chain of anisotropic spin-spin interactions. II. Properties of the ground-state energy per lattice site for an infinite system, *Phys. Rev.* **150**, 327 (1966).
- [77] C. N. Yang and C. P. Yang, One-dimensional chain of anisotropic spin-spin interactions. III. Applications, *Phys. Rev.* **151**, 258 (1966).
- [78] A. Langari, Phase diagram of the antiferromagnetic xxz model in the presence of an external magnetic field, *Phys. Rev. B* **58**, 14467 (1998).
- [79] H.-J. Mikeska and A. K. Kolezhuk, One-dimensional magnetism, in *Quantum Magnetism*, edited by U. Schollwöck, J. Richter, D. J. J. Farnell, and R. F. Bishop (Springer, Berlin, 2004), pp. 1–83.
- [80] T. Giamarchi, *Quantum Physics in One Dimension*, International series of monographs on physics (Clarendon Press, Oxford, 2004).
- [81] A. Peres, Separability Criterion for Density Matrices, *Phys. Rev. Lett.* **77**, 1413 (1996).
- [82] M. Horodecki, P. Horodecki, and R. Horodecki, Separability of mixed states: necessary and sufficient conditions, *Phys. Lett. A* **223**, 1 (1996).

- [83] G. Vidal and R. F. Werner, Computable measure of entanglement, *Phys. Rev. A* **65**, 032314 (2002).
- [84] K. Życzkowski, P. Horodecki, A. Sanpera, and M. Lewenstein, Volume of the set of separable states, *Phys. Rev. A* **58**, 883 (1998).
- [85] J. Lee, M. S. Kim, Y. J. Park, and S. Lee, Partial teleportation of entanglement in a noisy environment, *J. Mod. Opt.* **47**, 2151 (2000).
- [86] M. Horodecki, P. Horodecki, and R. Horodecki, Inseparable Two Spin- $\frac{1}{2}$ Density Matrices can be Distilled to a Singlet Form, *Phys. Rev. Lett.* **78**, 574 (1997).
- [87] W. Dür, J. I. Cirac, M. Lewenstein, and D. Bruß, Distillability and partial transposition in bipartite systems, *Phys. Rev. A* **61**, 062313 (2000).
- [88] W. Dür and J. I. Cirac, Activating bound entanglement in multiparticle systems, *Phys. Rev. A* **62**, 022302 (2000).
- [89] M. B. Plenio, Logarithmic Negativity: A Full Entanglement Monotone that is Not Convex, *Phys. Rev. Lett.* **95**, 090503 (2005).
- [90] C. H. Bennett, D. P. DiVincenzo, J. A. Smolin, and W. K. Wootters, Mixed-state entanglement and quantum error correction, *Phys. Rev. A* **54**, 3824 (1996).
- [91] C. H. Bennett, H. J. Bernstein, S. Popescu, and B. Schumacher, Concentrating partial entanglement by local operations, *Phys. Rev. A* **53**, 2046 (1996).
- [92] I. Bengtsson and K. Życzkowski, *Geometry of Quantum States: An Introduction to Quantum Entanglement* (Cambridge University Press, Cambridge, UK, 2006).
- [93] R. Banerjee, A. K. Pal, and A. Sen(De), Uniform decoherence effect on localizable entanglement in random multiqubit pure states, *Phys. Rev. A* **101**, 042339 (2020).
- [94] Xiao-yu Chen and Li-zhen Jiang, Noise tolerance of Dicke states, *Phys. Rev. A* **101**, 012308 (2020).
- [95] A. Sanpera, R. Tarrach, and G. Vidal, Local description of quantum inseparability, *Phys. Rev. A* **58**, 826 (1998).
- [96] S. Rana, Negative eigenvalues of partial transposition of arbitrary bipartite states, *Phys. Rev. A* **87**, 054301 (2013).
- [97] M. G. M. Moreno and F. Parisio, All bipartitions of arbitrary Dicke states, [arXiv:1801.00762](https://arxiv.org/abs/1801.00762) (2018).
- [98] R. Banerjee, A. K. Pal, and A. Sen(De), Hierarchies of localizable entanglement due to spatial distribution of local noise, *Phys. Rev. Res.* **4**, 023035 (2022).
- [99] P. Pfeuty, The one-dimensional Ising model with a transverse field, *Ann. Phys.* **57**, 79 (1970).
- [100] A. Osterloh, L. Amico, G. Falci, and R. Fazio, Scaling of entanglement close to a quantum phase transition, *Nature* **416**, 608 (2002).
- [101] T. J. Osborne and M. A. Nielsen, Entanglement in a simple quantum phase transition, *Phys. Rev. A* **66**, 032110 (2002).
- [102] P. Schindler, D. Nigg, T. Monz, J. T. Barreiro, E. Martinez, S. X. Wang, S. Quint, M. F. Brandl, V. Nebendahl, C. F. Roos, M. Chwalla, M. Hennrich, and R. Blatt, A quantum information processor with trapped ions, *New J. Phys.* **15**, 123012 (2013).
- [103] A. Bermudez, X. Xu, R. Nigmatullin, J. O’Gorman, V. Negnevitsky, P. Schindler, T. Monz, U. G. Poschinger, C. Hempel, J. Home, F. Schmidt-Kaler, M. Biercuk, R. Blatt, S. Benjamin, and M. Müller, Assessing the Progress of Trapped-Ion Processors Towards Fault-Tolerant Quantum Computation, *Phys. Rev. X* **7**, 041061 (2017).
- [104] H.-P. Breuer and F. Petruccione, *The Theory of Open Quantum Systems* (Oxford University Press, Oxford, 2002).
- [105] <https://github.com/titaschanda/QIClib>.